NOVEMBER 1997

GEOLOGIC MEMBRANE CONTROLS ON SATURATED ZONE HEAVY METAL TRANSPORT

WRRI Technical Completion Report No. 303

T. M. Whitworth
Gina DeRosa

NEW MEXICO WATER RESOURCES RESEARCH INSTITUTE
New Mexico State University
Box 30001, MSC 3167
Las Cruces, New Mexico 88003-0001
Telephone (505) 646-4337 FAX (505) 646-6418

GEOLOGIC MEMBRANE CONTROLS ON SATURATED ZONE HEAVY METAL TRANSPORT

By

T. M. Whitworth
Principal Investigator
New Mexico Bureau of Mines and Mineral Resources
New Mexico Tech

and

Gina DeRosa
Research Assistant
Department of Earth and Environmental Science
New Mexico Tech

TECHNICAL COMPLETION REPORT

Account Number 1423923

November. 1997

New Mexico Water Resources Research Institute

in cooperation with

New Mexico Bureau of Mines and Mineral Resources
New Mexico Tech

The research on which this report is based was financed in part by the U.S. Department of the Interior, Geological Survey, through the New Mexico Water Resources Research Institute.

DISCLAIMER

The purpose of the Water Resources Research Institute technical reports is to provide a timely outlet for research results obtained on projects supported in whole or in part by the institute. Through these reports we are promoting the free exchange of information and ideas, and hope to stimulate thoughtful discussions and actions which may lead to resolution of water problems. The WRRI, through peer review of draft reports, attempts to substantiate the accuracy of information contained in its reports, but the views expressed are those of the authors and do not necessarily reflect those of the WRRI or its reviewers. Contents of this publication do not necessarily reflect the views and policies of the Department of the Interior, nor does the mention of trade names or commercial products constitute their endorsement by the United States government.

ACKNOWLEDGMENTS

The authors would like to express appreciation to the New Mexico Bureau of Mines for providing matching funds for this project. Lynn Brandvold, Barbara Popp, and Sandy Swartz freely made the NMBMMR chemistry laboratory facilities available and assisted with the analyses. Chris McKee performed the X-ray fluorescence analysis and X-ray diffraction analysis in the NMBMMR X-ray lab. Mike Splide, Department of Meteoritics, University of New Mexico operated the microprobe for this project. Virgil Lueth, NMBMMR mineralogist/economic geologist took photomicrographs and otherwise helped in ways too numerous to mention. Judy Vaiza kept the budget and ordered necessary supplies. Karen Spiker and Matt Falkenstein contributed to this project in many ways as undergraduate research assistants.

ABSTRACT

When a clay membrane partially rejects solute, a concentration polarization layer (CPL) forms at the higher-pressure membrane interface. Solute concentrations at the membrane may be from several to more than 100 times that of background concentration. Therefore, even though the concentration outside the CPL may be below saturation, concentrations within the CPL nearest the membrane may reach supersaturation and precipitation may occur.

As an experimental test of this concept, seven hyperfiltration experiments were performed with sedimented clay membranes; three with undersaturated copper carbonate solutions, two with undersaturated lead chloride solutions, one with an undersaturated copper chloride solution, and two with undersaturated cobalt chloride solutions. Heavy metal precipitates were present during scanning electron microscopic examination of the clay membranes for six out of the seven experiments, and in two of these experiments heavy metal precipitate was visible to the naked eye through the clear acrylic cell before the experiments ended.

One problem with geologic membrane research is in obtaining measured values of the membrane coefficients quickly and efficiently. Several experiments were performed with two litho-osmometers. These instruments were designed to measure the membrane coefficients of shales. Preliminary results suggest that neither design works rapidly enough for routine commercial use.

An analytical, steady-state model was developed to predict when heavy metal precipitation due to membrane processes in the subsurface is possible. This model is adaptable for use at specific contaminated sites.

TABLE OF CONTENTS

LIST OF FIGURES

LIST OF TABLES

JUSTIFICATION OF WORK PERFORMED

Based on theoretical, non-equilibrium thermodynamic calculations, Whitworth and Lueth (1994) suggested that membrane-induced heavy metal precipitation might be an important process in contaminated zones. While some previous research has been done on the membrane properties of clays, no experimental work on clay membrane-induced precipitation of heavy metals has been performed prior to this study. However, the fact that a clay membrane can cause mineral precipitation was previously proven. In a landmark experimental study, Fritz and Eady (1985) precipitated calcite on a clay membrane by passing an undersaturated solution through the clay. Fouling of synthetic membranes by mineral precipitation is also a problem in reverse osmosis desalination (Merten et al. 1964; Strathmann and Kelinin 1969; Mitsoyannis and Saravacos 1977). In addition, field examination of sedimentary copper deposits in New Mexico, which also contain small amounts of silver, zinc, cadmium, and lead, suggests that some sedimentary ore deposits may be natural analogs of this process (Whitworth and Lueth 1994; Lueth and Whitworth 1994a).

The purpose of this research was threefold: 1) to demonstrate experimentally that membrane-induced precipitation of heavy metals can occur in the laboratory, 2) to attempt to develop a routine method for measuring membrane coefficients of shales, and 3) to develop a steady-state mathematical model which can be used to assess potential membrane effects at specific sites.

A major question concerning the role of shale membranes in the subsurface is what pressure differentials commonly exist across bounding aquitards? The answer to that question is outside the scope of this research. However, the pressure differential across bounding shales can be measured when needed at specific contaminated sites. The model developed in this research will predict both the lack of membrane effects as well as quantitatively define them when the needed parameters are input.

Geologic Membrane Processes

A semi-permeable membrane is defined as a material which will permit the passage of some molecules but not others (Noggle 1984). As defined, the membrane would be perfect, that is it would

absolutely preclude the passage of certain molecular species. Such perfect membranes probably do not exist in nature (Fritz 1986). Therefore, a better working definition for a semi-permeable, geological membrane is any lithology which retards one solution component more effectively than another.

Many studies have experimentally confirmed the ability of clays, which are a major component of shales, to act as semi-permeable membranes (Briggs 1902; Kohler 1903; Marshall 1948; Wyllie 1948, 1949; Kemper 1960, 1961; McKelvey and Milne 1960; Bernstein 1960; McKelvey and Milne 1963; Olsen 1969, 1972; Kemper and Rollins 1966; Kharaka and Berry 1973; Coplen and Hanshaw 1973; Srivastava and Jain 1975; Kharakra and Smalley 1976; Fritz and Marine 1983; Benzel and Graf 1984; Fritz and Eady 1985; Campbell 1985; Haydon and Graf 1986; Demir 1988; Fritz et al. 1987; Fritz and Whitworth 1994; Whitworth and Fritz 1994). In addition, Young and Low (1965) conducted experiments in which they passed saline solutions through actual discs of shale and siltstone. Their experiments demonstrated that shales and siltstone are capable of acting as semi-permeable membranes.

In addition to laboratory studies, many field studies have alluded to the existence of geologic membranes. For example, the Milk River aquifer in the western Canadian sedimentary basin has been cited as a field example of membrane processes (Berry 1960, Phillips et al., 1986), as have the Illinois Basin (Bredehoeft et al. 1963; Graf et al. 1965; Graf et al. 1966), the Imperial Valley in California (Berry 1966, 1967), the Oxnard coastal basin, Ventura County, California (Greenberg et al. 1973), the San Juan basin in northeastern New Mexico and southwestern Colorado (Berry 1959), the Paradox basin in Utah, Colorado, and New Mexico (Hanshaw and Hill 1969), the Wheeler Ridge anticline, San Joaquin Valley, California (Berry 1960), Kettleman North Dome, California (Kharaka, Berry, and Friedman 1973), and the Saginaw aquifer system, in the upper Grand River basin, Michigan (Wood 1976).

Membranes may reject solutes on the basis of size and/or electrical restrictions (Gregor and Gregor 1978). If a geological material has a net electrical charge, then electrical restrictions become important. For example, smectite clays have a net negative charge due to ion substitution in the lattice (Grim 1968).

In smectite membranes, the electrical restrictions contribute to solute rejection for charged species such as electrolytes. However, the net negative charge would have no direct effect on uncharged ion pairs or non-electrolytes in solution. In this case, separation is accomplished because the non-electrolyte species enter and traverse the membrane more slowly than the aqueous solvent. If a membrane material has no net charge, like kaolinite (Grim 1968), then electrolyte rejection must be primarily attributed to rejection on the basis of molecular size. Other physico-chemical processes such as adsorption and ion exchange are also important for certain membrane types (Sourirajan 1970).

Two types of membrane processes are believed to be common in the subsurface: osmosis and reverse osmosis (Graf 1982). Osmosis is the net flux of water and solute that results when two solutions of different concentration are separated by a membrane. The fluxes occur because both the water and the solute tend to flow from high to low concentration. This results in a net flux of solute from the more concentrated solution across the membrane to the less concentrated solution, and a net flux of water molecules in the opposite direction through the membrane. The osmotic pressure is defined as the pressure necessary to stop the flow of solute from high to low concentration across the membrane (Martin 1964).

Hyperfiltration (reverse osmosis) occurs when sufficient pressure is applied to the high-concentration membrane face to reverse the direction of water flow through the membrane. Under hyperfiltration conditions, both solute and water flow across the membrane from high to low solute concentration. Both osmosis and hyperfiltration can occur in the subsurface in conjunction with geologic membranes (Graf 1982).

There are two end-member scenarios which describe subsurface flow patterns associated with hyperfiltration. In the one-dimensional flow scenario, all of the flux is constrained to pass through the membrane (Fig. 1). Theoretically this situation begins with identical solute concentrations on both sides of the membrane at time t = 0 (Fig. 1A). Because water passes more easily through the membrane than the solute, as time passes the solute begins to accumulate at the high-pressure membrane face (Fig. 1B) The

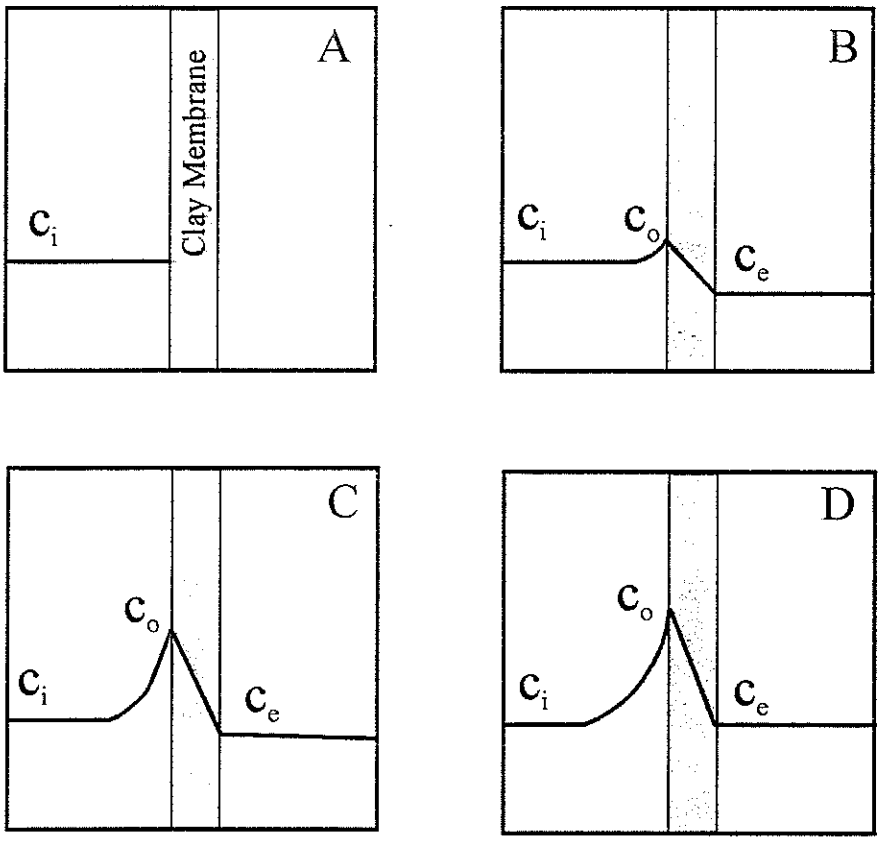

Figure 1. Conceptual development of the concentration polarization layer. The initial conditions (A) are such that the solute is all on the high pressure side of the membrane and the pore fluids within the membrane contain no solute. Some time after solute flux through the membrane begins (B) the concentration at the high pressure membrane face c_o increases because some of the solute is rejected by the membrane. Some solute also begins to pass through the membrane so that the effluent now contains some solute as well. Even later (C) c_o has increased further as has the effluent concentration c_e. At steady-state (D) the input concentration c_i is now equal to c_e and the value of c_o is constant. (Redrawn from Fritz and Marine 1983).

zone of increased concentration at the high-pressure membrane face is called the concentration polarization layer (CPL). As the CPL grows, ever more solute is available at the high-pressure membrane face to enter the membrane. Hence, membrane efficiency decreases and the effluent concentration tends to increase concurrently with growth of the CPL (Fritz and Marine 1983; Fritz 1986; Whitworth 1993; Fritz and Whitworth 1994). The concentration at the high-pressure membrane face continues to increase with time as does the width and amount of solute in the CPL (Fig. 1C). After sufficient time has passed, an equilibrium is reached (Fig. 1D) in which the effluent concentration stabilizes at that of the original input concentration. At equilibrium the CPL still exists, even though the membrane efficiency is zero, because there is no difference in the concentration of the input and effluent solutions. It should be noted at this point that some membranes may have low solute concentrations within the membrane and thus exhibit discontinuous concentration profiles unlike that shown in Figure 1 (Phillips 1983). However, all membranes when operated in one-dimensional flow, eventually reach an equilibrium where the input concentration is equal to the output concentration.

The second end-member scenario is that of the cross-flow cell (Fig. 2). This flow scenario is analogous to that used in reverse-osmosis desalination. In cross-flow desalination units, the high-pressure face of the membrane is swept by a high velocity flux designed to minimize the CPL development. Only a small portion of the total flux passes through the membrane. In the subsurface this might occur when the majority of the groundwater flow is directed along the aquifer and a much smaller flux is directed perpendicularly through the geological membrane. Because the CPL is diminished by the cross-component of flow, a quasi-equilibrium is reached in which the membrane efficiency is greater than zero. Membrane efficiencies as high as 99.8 % for NaCl removal have been reported for synthetic membranes operated in this configuration (Mariñas and Selleck 1992). However, due to low groundwater flow velocities, it is unlikely that the cross-component of flow in an aquifer could destroy the CPL as thoroughly as is done

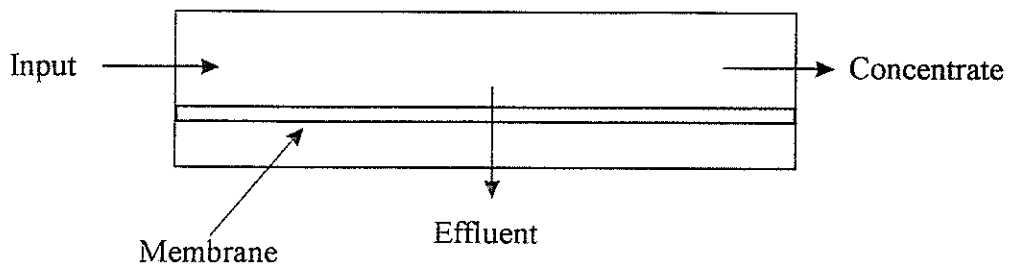

Figure 2. Schematic of a cross-flow cell. In commercial reverse osmosis the membrane is swept by a cross-flux designed to minimize the development of a CPL. As a result, only a small portion of the flux passes through the membrane. The solution which does not pass through the membrane becomes increasingly concentrated as it flows parallel to the membrane. An analogous situation in the subsurface occurs when groundwater flowing along a confined aquifer becomes increasingly concentrated along the flow path because a portion of the solute is retained by the shale membrane from the component of flow which passes through it. The figure shows no CPL development at the membrane. However, because groundwater flow velocities are relatively low, it is not likely that the CPL would be completely destroyed in the subsurface.

during commercial, reverse-osmosis desalination unless vertical gradients are very low. Rather, the effect should be to somewhat limit CPL development. Therefore, the one-dimensional flow scenario will be investigated in this research.

Natural Analogs of Membrane-Induced Precipitation

Whitworth and Lueth (1994), Lueth and Whitworth (1994a), and Lueth and Whitworth (1994b) examined two sedimentary copper districts in New Mexico and found that copper mineralization invariably occurred at sand-shale boundaries and that mineralization was always most intense nearest the shale and diminished with distance from the shale in both districts. In no case did significant mineralization extend into unfractured shales. In addition, mineralization tended to be greater adjacent to the thinner shales.

Based on these observations, they proposed that these deposits may form due to solute-sieving by the shales. A brief description of their proposed membrane model is as follows. Copper most likely enters solution through water-rock interaction when the fluid flows through rocks which are high in copper. The majority of the solution then flows along an aquifer bounded by confining shales. When groundwater passes through the shale membrane, a portion of the solute is rejected. If the volume flux toward the membrane is sufficient to prevent the rejected solute from completely diffusing back into the aquifer, a CPL forms. Concentrations within the CPL, near the membrane, can reach supersaturation thus encouraging copper mineral precipitation in the sandstone adjacent to the bounding shale units. Sulfate-reducing bacteria should be concentrated within the CPL as well and may participate in copper mineral precipitation. Because concentrations are the highest at the membrane interface and diminish into the aquifer, mineralization will be at maximum closest to the membrane and generally diminish with distance away from the membrane.

In the case where the flux toward the membrane is insufficient to prevent the rejected solute from diffusing back into the aquifer, no CPL will form. Therefore, where flux toward and through the membrane is very low, no copper mineralization is expected at the membrane interface. Mineralization should only occur where the CPL develops to where the solute concentration at the higher pressure membrane face is greater than solubility for a mineral species. This may explain why copper mineralization is not ubiquitous throughout the host rock and why mineralization favors the thinner shales where, for a given set of conditions, the solution flux through the shale is the highest. The observation that sedimentary copper deposits may form due to solute-sieving processes has significant implications for the potential fate of heavy metal contaminants in the subsurface.

Membrane Mathematics

A useful mathematical treatment of membrane phenomena is that of Kedem and Katchalsky (1962) and Katchalsky and Curran (1965). Fritz and Marine (1983) were the first to systematically apply this mathematical approach to geological membranes. Subsequent papers which further develop the application of this system of equations to geological membranes are: Fritz and Eady (1985), Fritz (1986), Fritz et al. (1987), Fritz (1992), Fritz and Whitworth (1993, 1994). The approach of Kedem and Katchalsky (1962), and Katchalsky and Curran (1965) is also commonly used in work with synthetic reverse osmosis desalination membranes (Spiegler and Kedem 1966; Harris et al. 1976; Pusch 1986; Mariñas and Selleck 1992; Whitworth et al. 1994).

The approach of Katchalsky and Curran (1965) is based on non-equilibrium thermodynamics. De Groot and Mazur (1962) state that non-equilibrium thermodynamics is a continuum theory which treats the state parameters as continuous functions of space coordinates and time. Therefore, non-equilibrium thermodynamics applies to both steady-state as well as smoothly changing transient conditions. Thus, the non-equilibrium thermodynamic approach should apply to most subsurface hydrological situations. There are, however, other mathematical descriptions of membranes including kinetic models, and the application of impedance, cable theory, and Hodgkin-Huxley equations (Lakshminarayanaiah 1984) and transient solutions by Greenberg and others (1973) and Fritz and Whitworth (1994). Other mathematical approaches used in reverse osmosis desalination are also discussed by Soltanieh and Gill (1981).

Kedem and Katchalsky (1962) derived two equations which describe the flow of solution and solute through membranes. These equations were developed for non-electrolytes, but have been successfully applied to electrolytes (Spiegler and Kedem 1966; Harris et al. 1976; Mariñas and Selleck 1992; Whitworth et al. 1994). As presented here, these equations describe a single solute system with no precipitation occurring at the membrane. The two equations are:

$$J_v = L_p(\Delta P - \sigma\Delta\pi) \qquad (1)$$

and

$$J_s = \bar{c}_s(1-\sigma)J_v + \omega\Delta\pi \tag{2}$$

Where J_v = solution flux (cm/s) through the membrane, L_p = water permeation coefficient (cm^3/dyne·s), ΔP = pressure difference across the membrane (dyne/cm^2), σ = reflection coefficient (dimensionless), $\Delta\pi$ = theoretical osmotic pressure difference across the membrane (dyne/cm^2), J_s = solute flux (mole/cm^2·s) through the membrane, ω = solute permeation coefficient (mole/dyne·s), and $\bar{c}_s$ = average solute concentration across the membrane in mole/cm^3 where

$$\bar{c}_s = \frac{c_o + c_e}{2} \tag{3}$$

where c_o = concentration at the high-pressure membrane face (mole/cm^3) and c_e = effluent concentration (mole/cm^3).

An approximate equation for $\Delta\pi$ for a dilute single solute is

$$\Delta\pi = vRT(c_o - c_e) \tag{4}$$

Where v is a factor that corrects for the number of particles due to ion formation. For example, since NaCl forms two ions in solution, Na^+ and Cl^-, then for NaCl, v = 2. However, for $CaCl_2$, which forms one Ca^{++} ion and two Cl^- ions for each molecule of $CaCl_2$, v = 3. In Equation 3, R is the gas constant (8.314×10^7 dyne·cm/mole·°K) and T is the temperature in °K.

Fritz (1986) suggested that three of the phenomenological coefficients of Katchalsky and Curran (1965)—σ, ω, and L_p—are useful in describing the behavior of non-ideal, geologic membrane systems. First, consider the reflection coefficient σ, which was first defined by Staverman (1952). Permissible values of σ range from zero to one. If $\sigma = 0$, then there is no membrane effect. In this case Equation 1 reduces to $J_v = L_p\Delta P$, which is a one-dimensional form of Darcy's Law. If $\sigma = 1$, the membrane is ideal and no solute can pass through the membrane. The value of σ for non-ideal geological membranes must be

greater than zero, but less than one. Fritz and Marine (1983) calculated values of σ for a series of six experiments using bentonite clay membranes compacted to different porosities and NaCl solutions. The values of σ they determined ranged from 0.04 to 0.89. Fritz and Marine (1983) state that σ is important because it is a measure of the osmotic efficiency of a membrane. Thus, a membrane with a $\sigma = 0.90$ would exhibit 90 % of the theoretically predicted osmotic pressure. For solutes such as NaCl, with identical anion and cation concentrations, $\sigma_{anion} = \sigma_{cation}$. However, for systems such as $CuCl_2$, where the dissolved anion concentration is twice that of the cation concentration, the anion and the cation have differing values of σ.

The solute permeation coefficient ω describes the diffusion of solute through the membrane. For ideal membranes, $\omega = 0$ because no solute can pass through the membrane. For typically non-ideal geologic membranes ω should be greater than zero. Elrick and others (1976) measured ω for a Na-bentonite slurry with 90 % porosity and obtained a value of 3×10^{-15} mole/dyne·s. Fritz and Marine (1983) suggested that for more compacted bentonites, the value of ω should be considerably lower than 3×10^{-15}. Similarly, for systems where the anion concentration is not equal to the cation concentration, $\omega_{anion} \neq \omega_{cation}$.

The water permeation coefficient L_p is related to the hydraulic conductivity K (in cm/s) by the expression (Fritz 1986)

$$L_p = \frac{K}{\rho g x} \tag{5}$$

where ρ is the fluid density in g/cm^3, g is the gravitational constant in cm/s^2, and x is the membrane thickness in cm. In general, as L_p decreases, membrane efficiency increases.

Fritz and Marine (1983) derived a steady-state solution which describes the CPL profile within the free solution abutting the membrane. Their equation is

$$c_x = (c_o - c_i)\left[\exp(\frac{-J_v x}{D}) - \exp(\frac{-J_v x_i}{D})\right] + c_i \quad (6)$$

Where c_x is the concentration in moles/cm^3 at distance x (cm) from the membrane, and x_i is the distance from the membrane where $c_x = c_i$ and D is the solute diffusions coefficent in cm^2/s. In Equation 6, J_v represents the flux toward the membrane.

Fritz and Whitworth (1994) state that the term $-\exp(-J_V x_i/D)$ in Equation 6 can be ignored if the length of the test cell is large relative to the ratio D/J_V. However, diffusion in free solution occurs more rapidly than diffusion in porous media due to interaction of the diffusing solute with the mineral grains (Fetter 1988; Domenico and Schwartz 1990). The effective solute diffusion coefficient for porous media is typically represented by D* (Freeze and Cherry 1988; Fetter 1988). D* is defined by the relation $D^* = wD$, where w is a unitless empirical constant determined from laboratory experiments (Fetter 1988). Freeze and Cherry (1988) reported that w ranges from 0.01 to 0.5. The lower end of this range is for clayey sediments (Berner 1971). This term can also be ignored if the thickness of the aquifer is large relative to the ratio D^*/J_V. Therefore, for porous media, Equation 6 reduces to

$$c_x = (c_o - c_i)\left[\exp(\frac{-J_v x}{D^*})\right] + c_i \quad (7)$$

Here D* is substituted for D as discussed earlier.

Fritz and Marine (1983) stated that because ω tends to be very small, the $\omega\Delta\pi$ term in Equation 2 can often be ignored. By omitting the $\omega\Delta\pi$ term and by substituting Equation 3 into Equation 2, they derived the following relationship

$$\sigma \approx \frac{c_o - c_e}{c_o + c_e} \quad (8)$$

It was previously stated that, at equilibrium for a static cell configuration, $c_e = c_i$, therefore, by substituting c_i for c_e into the above relationship and solving for c_o we can develop the following approximate relationship between σ, c_i, and c_o

$$c_o \approx \frac{-(\sigma c_i + c_i)}{\sigma - 1} \tag{9}$$

Using Equation 8, and plotting values of σ versus c_i yields a graph of σ versus c_o/c_i (Fig. 3). For example, for a sigma of 0.55, as obtained by Fritz and Whitworth (1994), the graph shows that the c_o/c_i ratio should be about 3.45. This is very close to the value of 3.48 obtained by Fritz and Whitworth (1994) at equilibrium for their static cell membrane experiment.

The smectite membrane used by Fritz and Whitworth (1994) was initially compacted to 34.5 bars (500 psi). Assuming the water table is shallow, the depth where the effective stress is roughly equivalent to 34.5 bars is 299 meters (983 feet). At depths of greater than 300 meters, we assume that greater compaction of clays and shales might yield values of σ greater than the 0.55 obtained by Fritz and Whitworth and therefore, the membrane concentration process may be even more effective with increasing depth. Of course, as Fritz (1986) pointed out, lithology also plays an important role in membrane efficiency. Smectites, with the smaller particle size, should be more efficient membranes at the same level of compaction, than kaolinites.

METHODS

Experimental Design for Precipitation Experiments

The experimental procedure consisted of forcing undersaturated copper carbonate and various metal chloride solutions through compacted smectite membranes and periodically collecting effluent samples. A syringe pump was used to force the solutions through the membranes at a constant solution flux. Figure 1 shows the experimental setup. The ISCO Model 500D syringe pump used in the

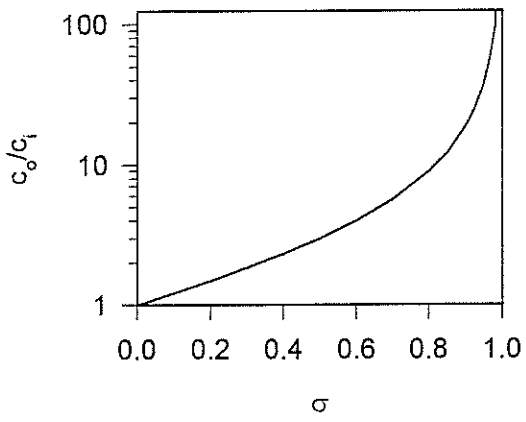

Figure 3. Relationship between the ratio of the solute concentration at the high-pressure membrane face and the background solute concentration within the aquifer (c_o/c_i) and the reflection coefficient σ. This diagram shows that the ability of a membrane to concentrate solutes increases as σ increases.

experiments has a 500 ml capacity and is capable of delivering fluid at constant rates ranging from 1.0 μ l·min^{-1} to 80 ml·min^{-1}, or at constant pressure up to an applied maximum of 258 bars.

The experimental hyperfiltration cell consists of a transparent acrylic cylinder with an internal diameter of 5.02 cm, and a wall thickness of 0.64 cm, which is fitted to two o-ringed, 3.8 cm thick, Garlite™ caps. The caps are held in place by eight threaded rods which pass through both caps parallel to the cylinder. A flat gasket provides the seal between the cylinder and the membrane. This is the same experimental cell design used by Fritz and Whitworth (1994) and is capable of operating at a working pressure of 68 bars (1000 psi). The hyperfiltration cell components were acid-washed and then rinsed with deionized water before each experiment.

Smectite was chosen to construct the membrane because most of the experimental work to date has been conducted with smectite (Kharaka and Berry 1973; Benzel and Graf 1984; Kharaka and Smalley 1976; Haydon and Graf 1986; Demir 1988; Coplen and Hanshaw 1973; McKelvey and Milne 1960; Fritz

et al. 1987; Fritz and Eady 1985; Fritz and Marine 1983; Campbell 1985), and because smectite has significant double layer properties. A commercial bentonite was used to prepare the smectite membranes. This upper Cretaceous clay was mined in Crook county, near Colony, Wyoming. X-ray analysis shows the clay used in these experiments to be an almost pure Na-smectite containing only a trace of quartz. The clay used to construct the membranes was beneficiated to achieve an average 30mm size by means of an air separator (Whitworth et. al. 1993). Following separation, the fine fraction was slurried with one molar NaCl solution, dialyzed to remove excess solute, and finally freeze-dried. To form the membranes, 0.60 grams of freeze-dried clay was slurried in approximately 200 ml of deionized water. This slurry was then placed in the experimental cell and connected to the syringe pump which was filled with deionized water. The syringe pump was then used to force the clay slurry through the experimental cell thus sedimenting the clay onto the filter paper at the base of the cell as a clay membrane. In each case fluid pressures of 1000 psi were used to compact the membrane. The entire process of building and compacting the membrane typically took between six and 18 hours. After the membranes were formed and compacted, deionized water was pumped through the clay membrane so that the filtration coefficient L_P could be measured. Following measurement of L_P, the deionized water was poured from the cell and replaced with the appropriate stock solution. Reagent grade chemicals were used to make the solutions. The syringe pump was then acid washed with 5% HNO_3 times, and then filled and flushed with the stock solution three times for each experiment to assure no contamination remained from previous uses.

Due to the length of the experiments and the dry climate, evaporation was a potential problem. Therefore, an evaporation control system (Fig. 4) was used to prevent evaporation of the effluent during the experiments. A rubber stopper was placed into the sample flask. Two tubes passed through the stopper. One was the effluent line which was connected to the membrane cell. The other was a capillary tube which also passed through another rubber stopper inserted into a second flask. The end of this capillary tube remained below the liquid level in the second flask. Another short length of capillary tube was inserted into

the stopper in the second flask and was open to the atmosphere. The feed solution tanks remained tightly sealed throughout the experiments. The ISCO syringe pump is equipped with a pressure transducer at the factory. The precision of this transducer is approximately ± 1.0 %.

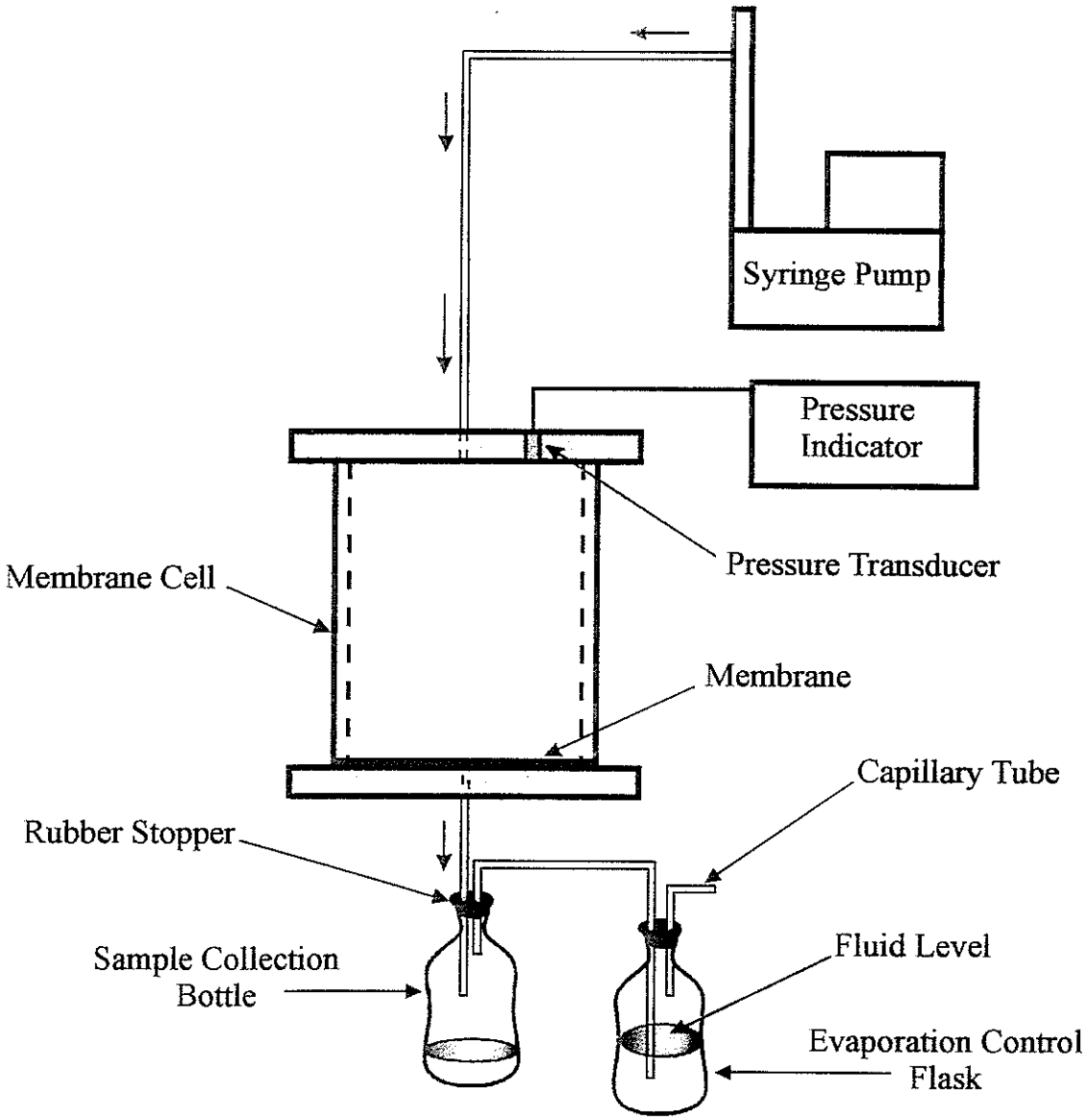

Figure 4. Experimental setup used for the precipitation experiments in this study.

PEEK (polyetheretherketone) tubing with an internal diameter of 0.159 cm was used to connect the membrane cell and the syringe pump. This plastic tubing has a burst strength of 345 bars. Stainless steel Swagelock® fittings and valves were used throughout to limit potential corrosion. A single monel fitting was accidentally used in the first three experiments. It was removed and replaced with a stainless steel fitting in subsequent experiments. The syringe pump has a volume of 500 ml. Therefore, it was necessary to refill the pumps periodically during the experiments. The procedure for refilling a syringe pump was as follows. First, the pump was valved-off from the cell so that the cell remained under pressure. Next, the pressure was relieved on the pump, it was refilled with stock solution, and then the pump was brought back up to pressure before the valve connecting it to the membrane cell was opened. The refill process typically took less than three minutes.

Effluent samples were collected periodically for analysis. The 125 ml or 60 ml Nalgene® sample bottles were acid washed with a 5% HNO_3 solution, rinsed several times with deionized water, and allowed to dry while covered to prevent dust contamination. The containers were then weighed (without caps) and the weights recorded to two decimal places. These sample bottles were used to collect the effluent samples. Approximately 1 ml of concentrated HNO_3 was added to a second set of similarly prepared set of sample bottles so that a portion of the collected effluent could be acidified and stored for subsequent metals analysis. The volume of each effluent sample was gravimetrically determined and pressure was periodically recorded. Following completion of an experimental run, the cell solution was stirred to homogenize it, saved, and analyzed to determine if any concentration increase occurred in the cell.

Each membrane was removed from the cell at the end of the experiment, flushed carefully and repeatedly with ethanol to remove any remaining water, and examined by scanning electron microscopy and electron microprobe energy dispersive analysis for precipitates. Analysis of the samples was carried out in a JEOL 733 Electron Microprobe at the University of New Mexico, Department of Earth and Planetary Science/Institute of Meteoritics. The microprobe has five tunable wavelength dispersive spectrometers

(WDS) and a Link Analytical thin-window energy dispersive spectrometer (EDS), controlled by an Oxford eXL II X-ray analytical system. The membranes were stored in custom built, acrylic containers. These containers consisted of two four-inch diameter by one-inch thick turned disks, one with a 4-mm deep recess to hold the membrane and attached filter paper, which were sealed together with silicon stopcock grease.

All stock solutions were prepared by mixing a saturated solution, filtering it through a 0.2 μm filter to remove suspended solids, and then diluting the required amount with deionized water.

Experimental Design of Litho-Osmometers

We tried two litho-osmometer designs. The first design was a stirred cell osmomometer. This device is similar to one first used by Walter (1982). Our modification of Walter's design is shown in Figure 5. The experimental procedure involved slicing a wafer off of a shale core and placing it in the apparatus. A vacuum was then pulled on the apparatus to displace the air in the osmomometer. Deionized water was then introduced to the deaired system while still under vacuum. Then the permeability (Lp) was measured by connecting the cell to a source of constant fluid pressure (syringe pump or constant head apparatus). The osmomometer chambers were then filled with the solutions of interest.

After the solutions of interest were placed into the stirred osmomometer cells, the levels in the manometer tubes were adjusted so that they were equal. The elevation of the solution levels in each manometer tube was then recorded at intervals (to the nearest mm) until steady-state was reached. Then from knowledge of Lp (from the run with Deionized water), Δx (measured), ΔP (from the manometer tubes), c_o, and c_i (from the initial solution concentrations), and the temperature, values of σ and ω can be calculated from equations 1 and 2.

The second design was based on a diffusion osmometer used for synthetic membranes (Shoemaker et al. 1981). The osmometer consists of a cylindrical cell with two ports (Fig. 6). One of these ports is attached to the syringe pump and the flow through the other port is controlled by a ball valve. The two

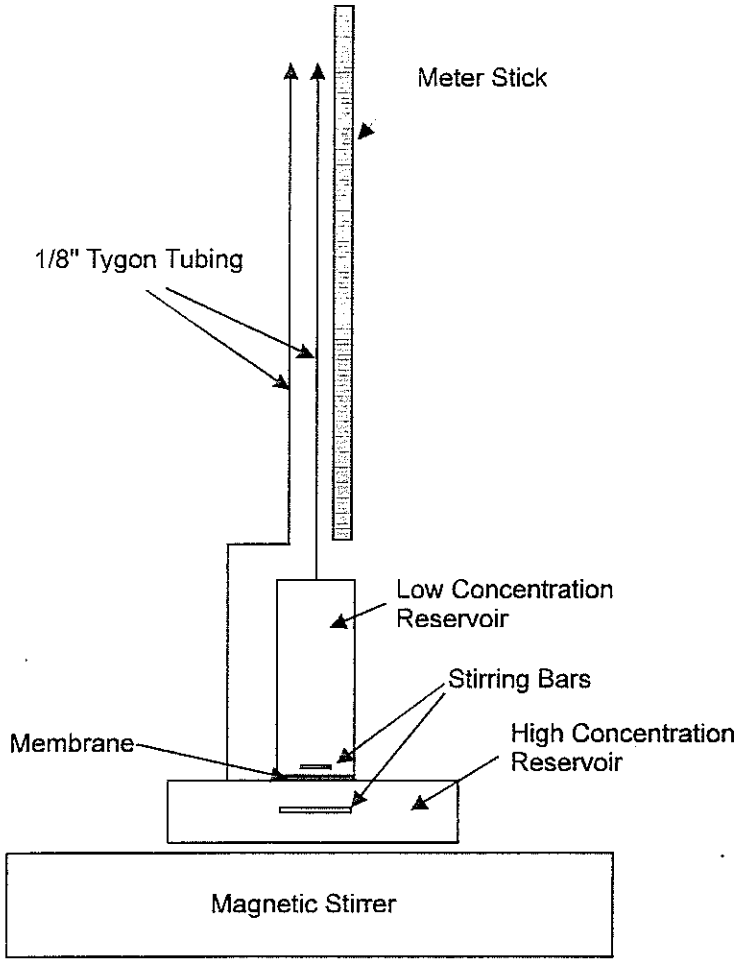

Figure 5. Schematic of experimental litho-osmometer apparatus for measuring membrane properties of shales. The shale wafer is held in place with gaskets to prevent leaks and to allow adjustment for different thickness wafers.

open ends of the cell have machined recesses into which fit thin disks of shale. These disks each seal against an o-ring and are held in place with larger perforated acrylic disks bolted into place. Coarse filter paper was placed between the perforated disks and the shale to more evenly distribute diffusive flow through the shale.

The procedure consisted of placing the shale disks into the lithosmometer and immersing it in a temperature-controlled bath of deionized water. The chamber was then filled with deionized water from the syringe pump. Care was taken to ensure no air bubbles remained in the cell and the other port was valved off. The syringe pump was then set to a constant pressure (usually 50 to 100 psi) and water was allowed

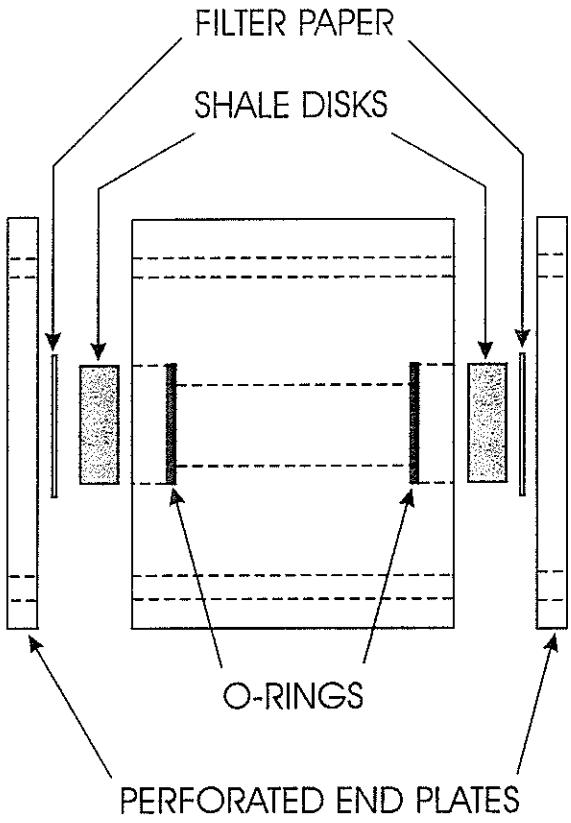

Figure 6. Second litho-osmometer experimental design.

to flow through the shale for several days. Then, the deionized water was displaced from the cell with the salt solution. Effluent conductivity was monitored to ensure that all of the deionized water was removed before valving off the effluent port. Then the cell was pressured to the target pressure (usually between 50 and 100 psi). The syringe pump was turned off and deadheaded into the system. The pressure decay was then monitored over time to see if it approached a steady-state. Next, the pressure was bled off and the system was repressured to a point below the last recorded pressure. The system was then locked off and the pressure was monitored to see if it would climb to the previous apparent steady-state pressure. This is

the Fuoss-Mead method of half sums (Shoemaker et al. 1981). By calculating one half the sum of the ordinates of the falling and rising pressure curves, one can obtain another curve which converges to a constant value. Correction for head differences between the transducer position and the cell position is necessary. Since water is essentially incompressible at the relatively low pressures used in these experiments, only a small amount of fluid is transferred across the membrane due to pressure changes and the concentrations can be assumed to be the starting concentrations.

Chemical Analyses

Acidified effluent samples were analyzed by both flame atomic absorption and graphite furnace atomic absorption methods. Standards for metals analysis were prepared from recently purchased, high purity, NBS traceable standards. Anions were analyzed titrimetrically using a Hach digital titrator. Periodic triplicate analyses served to determine the reported precision for each analytical method. The analytical precision for each type of analysis is reported in Table 1.

Table 1. Analytical precision of analyses.

Graphite Furnace Atomic Adsorption:
copper, ± 23% at 2 standard deviations
chrome, ± 10.6% at 2 standard deviations
manganese, ± 8.1% at 2 standard deviations
iron, ± 25% at 2 standard deviations
nickel, ± 37% at 2 standard deviations
Chloride titrations are ± 1.0 % at two standard deviations
Alkalinity Titrations are ± 2% at two standard deviations
Lead by flame AA (Experiment WRRI6) is 0.8% at two standard deviations
Lead by Flame AA (Experiment WRRI5) is 2.7% at two standard deviations.
Copper by flame AA is 3.3% at two standard deviations
Cobalt by flame AA is ± 1.3% at two standard deviations

RESULTS

Introduction

Seven hyperfiltration experiments with sedimented clay membranes were performed for this study; three with copper carbonate solutions, two with lead chloride solutions, one with a copper chloride solution, and one with a cobalt chloride solution. Of these seven experiments, six produced heavy metal precipitation and one apparently failed to produce heavy metal precipitation (Table 2). After the results of each experiment are presented, the mathematics necessary to calculate the membrane coefficients for each experimental run is derived and the results of the calculations are presented.

Table 2. Summary of hyperfiltration experiments.

Experiment	Solution	Results
WRRI2	80% $CuCO_3$	Mineral precipitation observed on scanning electron microscope
WRRI4	80% $CuCO_3$	Mineral precipitation observed on scanning electron microscope
WRRI5	80% $PbCl_2$	Mineral precipitation visually observed during experiment
WRRI6	23% $PbCl_2$	Mineral precipitation visually observed during experiment
WRRI7	80% $CuCO_3$	No mineral precipitation observed on scanning electron microscope
WRRI8	80% $CuCl_2$	Mineral precipitation visually observed during experiment
WRRI9	80% $CoCl_2$	Mineral Precipitation visually observed at end of experiment

Experiment WRRI2

The first attempt used a Na-montmorillonite pretreated with copper chloride solution to load the exchange sites with copper ions prior to the experiment. The clay was then dialyzed to remove excess copper ions and then oven-dried at 105°C. The oven-dried, copper-treated clay proved very difficult to re-

hydrate and did not disperse sufficiently in solution to form a membrane when sedimented on the filter paper. The fluid pressure never rose above zero during the run. Therefore the run was aborted and sodium-treated montmorillonite was used in this and subsequent experiments. Six-tenths of a gram of clay was sedimented onto filter paper in the experimental cell and compacted under 68 bars (1000 psi) of fluid pressure (Table 3) to form a membrane. The same compaction pressure was used in each subsequent experiment. The flow rate through the membrane was initially set at 150 ml/hr. However, the pressure in the cell rose rapidly to 46.8 bars (688 psi) by the time the sixth effluent sample was taken. Therefore, the flow rate was decreased to 100 ml/hr for the remainder of the experiment. The room temperature varied between 21.9 and 20.3 °C over the course of the experiment.

The input alkalinity was 0.122 mN and the alkalinity of the cell was 0.195 mN (Table 4). This suggests an alkalinity increase of 37.4 % in the cell at the close of the experiment relative to the input solution. The significantly increased alkalinity in the cell solution suggests that the sedimented clay was acting as a relatively efficient membrane.

The copper concentration of the input solution was 457 ppb (Table 4). The copper concentration of the cell solution at the end of the experiment was 472 ppb. Considering the 3.3% analytical precision for these analyses, there is no measurable difference in the copper concentrations in the input solution and in the cell. The copper concentration of the effluent began at 5.5 ppb in the first sample and slowly rose to only 20 ppb in the last effluent sample. Less than three percent of the copper advected toward the membrane exited the experimental cell in the effluent. Theoretically, at steady-state with no precipitation or ion exchange occurring, the copper concentration of the effluent should be equal to that of the input solution. Therefore, either steady-state was not reached, precipitation of copper was occurring on the high-pressure side of the membrane, significant ion exchange was occurring within the clay membrane, or some combination of these effects occurred. Alternatively, the fact that the average cell solution concentration was not greater may be due to the narrow CPL. In this and the other experiments, the CPL extended only a

Table 3. Data for experiment WRRI2.

Sample No.	Date	Sample Interval (hours)	Total Elapsed Time (hours)	Sample Volume (cm^3)	Total Volume Collected (cm^3)	ΔP (bars)	pH
WRRI2-1	1-13-96	--	--	--	--	--	5.95
WRRI2-2	1-13-96	0.767	0.767	107.0	107.0	17.86	5.96
WRRI2-3	1-13-96	0.700	1.467	110.1	217.1	21.65	5.96
WRRI2-4	1-13-96	0.767	2.234	115.3	332.4	25.44	6.00
WRRI2-5	1-13-96	0.850	3.084	124.3	456.7	29.23	5.79
WRRI2-6	1-13-96	0.800	3.884	119.2	575.9	47.44	5.61
WRRI2-7	1-13-96	1.067	4.951	120.8	696.7	30.13	5.59
WRRI2-8	1-13-96	1.283	6.234	129.2	825.9	30.27	5.49
WRRI2-9	1-13-96	1.133	7.637	113.5	939.4	30.89	5.55
WRRI2-10	1-13-96	1.300	8.667	127.8	1067.2	26.89	5.37
WRRI2-11	1-13-96	1.117	9.784	112.3	1179.5	27.65	5.67
WRRI2-12	1-13-96	1.183	10.967	118.0	1297.5	28.34	5.69
WRRI2-13	1-13-96	1.067	12.034	105.5	1403.0	28.48	5.77
WRRI2-14	1-13-96	1.167	13.201	112.7	1515.7	28.34	5.68
WRRI2-15	1-13-96	1.167	14.368	117.0	1632.7	29.03	5.89
WRRI2-16	1-14-96	1.167	15.535	116.2	1748.9	29.51	5.33
WRRI2-17	1-14-96	1.167	16.702	115.8	1864.7	29.99	5.80
WRRI2-18	1-14-96	1.200	17.902	117.7	1982.4	30.75	5.67
WRRI2-19	1-14-96	1.167	19.069	116.4	2098.8	31.37	5.56
WRRI2-20	1-14-96	--	--	--	--	--	6.47
WRRI2-21	1-14-96	--	--	--	--	--	6.16

Table 4. Chemical analyses for experiment WRRI2.

	Chemical Analyses (performed by graphite furnace atomic absorption spectrometry unless otherwise noted)								
Sample No.	HCO_3^{2} (mN)	Cu (ppb)	Cr (ppb)	Ni (ppb)	Fe (ppb)	Mn (ppb)	Na	Ca	Comments
WRRI2-1	0.122	457[1]	0.8	2.8	19	1.6	0[1]	0[1]	Pump Solution
WRRI2-2	0.097	5.5	0.6	5.9	15	0	0[1]	0[1]	
WRRI2-3	0.090	3.6	0.5	0.6	10	0	0[1]	0[1]	
WRRI2-4	0.089	5.5	0.5	0.5	11	0	0[1]	0[1]	
WRRI2-5	0.086	4.8	0.4	1.0	14	0	0[1]	0[1]	
WRRI2-6	0.077	4.6	0.5	0.5	8	0	0[1]	0[1]	
WRRI2-7	0.069	4.8	0.6	0.7	14	0	0[1]	0[1]	
WRRI2-8	0.068	5.0	1.0	1.0	7	0	0[1]	0[1]	
WRRI2-9	0.067	5.5	0.5	0.6	11	0	0[1]	0[1]	
WRRI2-10	0.060	5.3	0.4	0.5	8	0	0[1]	0[1]	
WRRI2-11	0.067	9.3	0.5	0.6	6	0.3	0[1]	0[1]	
WRRI2-12	0.059	7.1	0.4	0.5	5	0.2	0[1]	0[1]	
WRRI2-13	0.059	8.4	0.6	0.6	6	0.4	0[1]	0[1]	
WRRI2-14	0.058	8.0	0.5	0.6	7	0.7	0[1]	0[1]	
WRRI2-15	0.059	9.0	0.6	0.7	15	2.4	0[1]	0[1]	
WRRI2-16	0.075	9.3	0.5	0.6	17	2.7	0[1]	0[1]	
WRRI2-17	0.081	10.8	2.9	0.7	13	3.0	0[1]	0[1]	
WRRI2-18	0.063	11.5	0.5	0.7	7	3.8	0[1]	0[1]	
WRRI2-19	0.051	20.0	0.8	1.3	8	3.4	0[1]	0[1]	
WRRI2-20	0.107	443[1]	0.2	2.8	6	0.7	0[1]	0[1]	Pump Solution
WRRI2-21	0.195	472[1]	1.5	11.1	42	1.6	0[1]	0[1]	Cell Solution

[1]analyses by flame atomic absorption
[2]analyses by titration

short distance into the cell (typically less than 1.0 cm). Therefore, a truly representative sample of the cell solution may have been difficult to collect. The fact that the copper concentration within the cell was not higher than recorded might also be attributed to ion exchange or adsorption by the clay or copper mineral precipitation. The clay used in these experiments is a Na-treated smectite (montmorillonite) and smectites are noted for high exchange capacities. Therefore, it is likely that ion exchange is an important reason for

the low copper concentrations in the effluent. However, flame atomic absorption analysis of the WRRI2 samples for sodium showed none present in the samples. The detection limit for this method is 5 ppb. Therefore, ion exchange does not seem to play a major role in reducing the copper concentration of the effluent. Flame atomic absorption analysis of the effluent samples for calcium showed there was no measurable calcium in the effluent. However, the detection limit for calcium was 0.75 ppm. Therefore, the calcium analyses were inconclusive and it is possible that the calcium ion may have played a role in ion exchange.

Examination of the sedimented clay membrane after the experimental run on the scanning electron microscope and qualitative energy dispersive analysis on the microprobe shows that particles present on the membrane included a nickel-copper co-precipitate (containing minor amounts of Mn), iron sulfate, iron oxide, and calcium carbonate. Example graphs of the energy dispersive analyses of some of these particles are presented in figures 7, 8, and 9. Some of these particles displayed crystallinity, however, most appeared amorphous. Since carbon was used as the coating material, analysis of the carbonate phase is tenuous.

We were surprised to find nickel in the precipitates because there was none listed in the analysis of the copper carbonate we used to make our solution (Table 5). We then requested an analysis of the Isco syringe pump cylinder from the manufacturer (Table 6) because we suspected leaching of metals from the syringe pump walls. The syringe pump contains no copper. However, we did have a single monel swagelock fitting in line between the syringe pump and the experimental membrane cell on this experiment. Therefore, we also suspected that some of what we were seeing might be monel shards from that filling. Monel ranges from 65% Ni, 32% Cu, 2% Fe to 65% Ni, 30% Cu, 2% Fe, 3% Al + Ti (Oberg et al. 1992). The Ni-Cu ratio ranges from 2.0 to 2.2 for monel. However, the Ni-Cu ratio in the particles found on the membrane was approximately 2.8. Because we suspected that the nickel source might be dissolution from the syringe pump cylinder, we analyzed the pump solution for nickel, chrome, manganese, and iron by

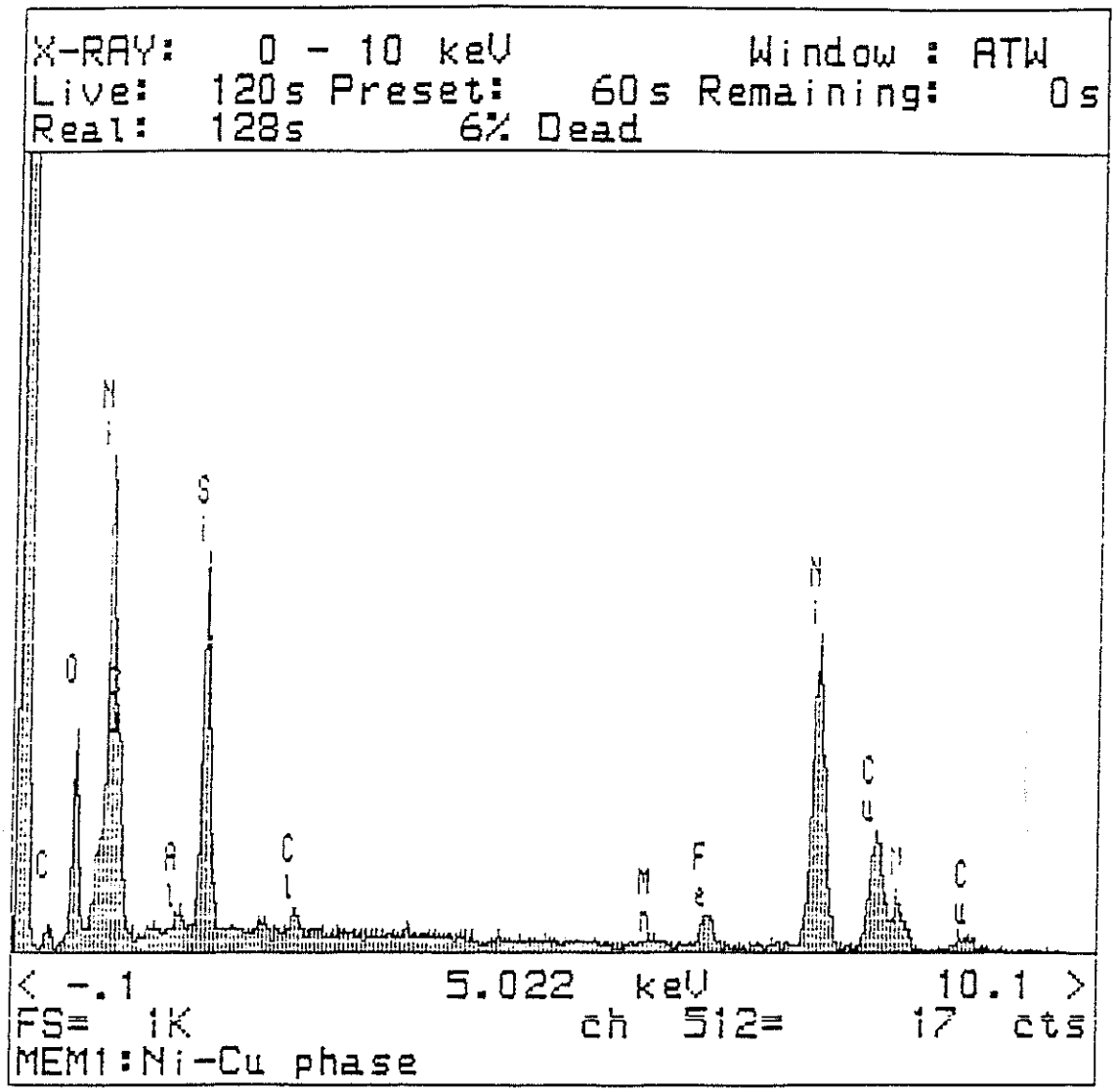

Figure 7. Energy dispersive spectra of Ni-Cu particle present on the surface of the membrane after experiment WRRI2. A number of these Ni-Cu particles were observed.

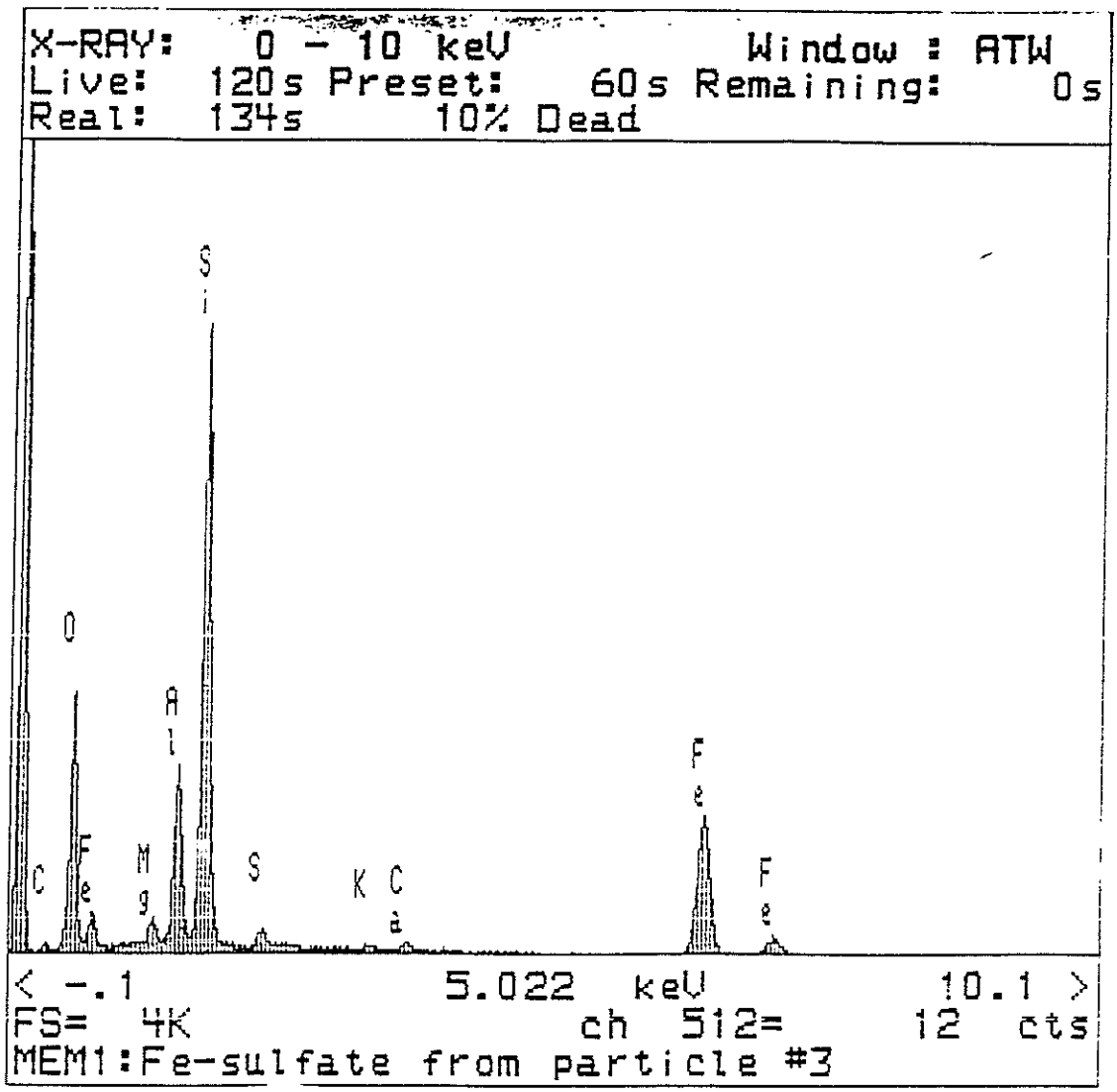

Figure 8. Energy dispersive spectra of iron sulfate particle present on the surface of the membrane after experiment WRRI2. This is the only iron sulfate phase observed.

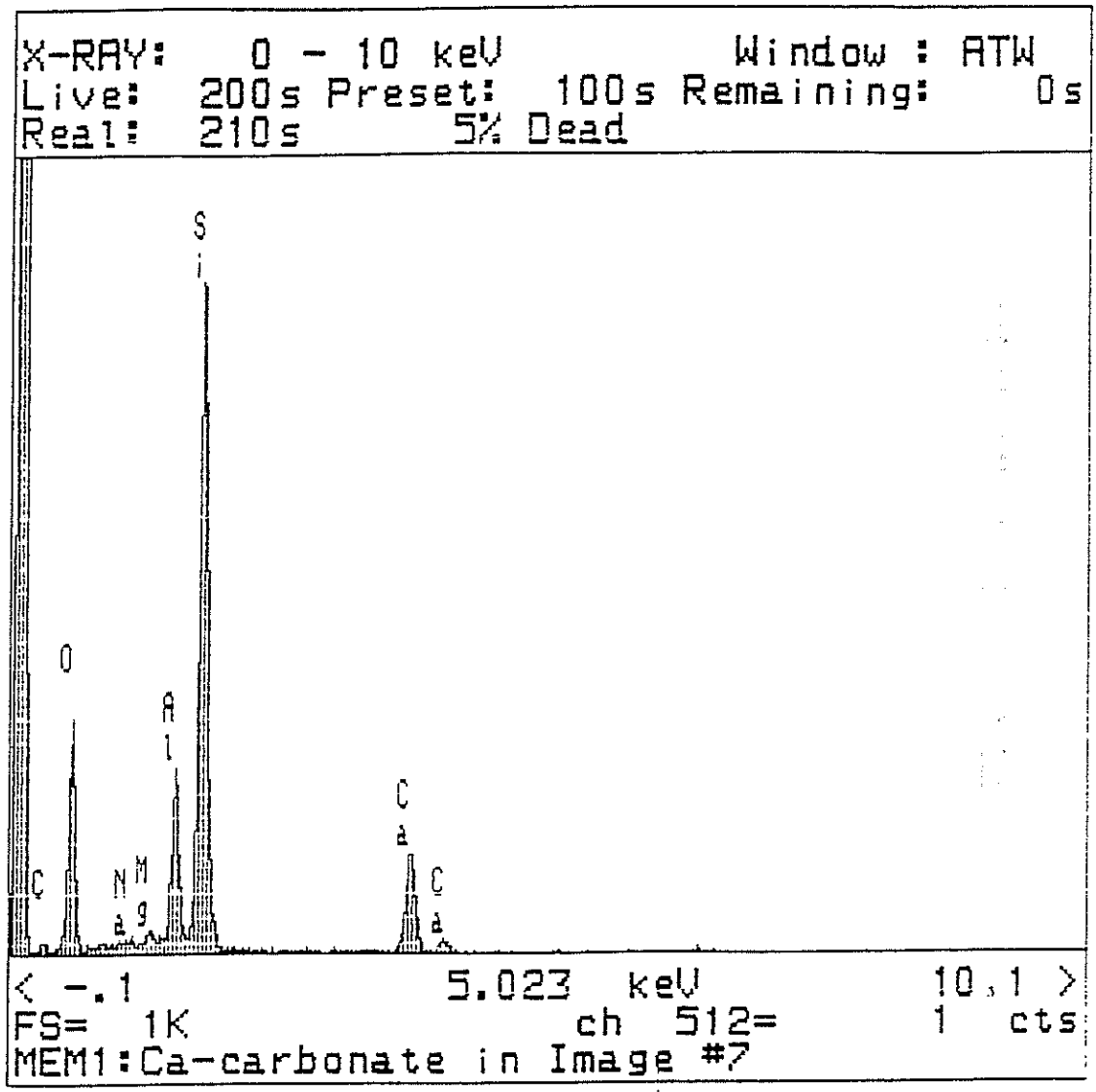

Figure 9. Energy dispersive spectra of calcium carbonate particle present on the surface of the membrane after experiment WRRI2. This is the only calcium carbonate phase observed.

Table 5. Analysis of lot F52333, J. T. Baker copper carbonate used in this study.

Component	Amount Present
Assay (as Cu)	56.2 %
Insoluble in HCl	< 0.005 %
Chloride (Cl)	< 0.001 %
Nitrate (NO_3)	0.03 %
Sulfate (SO_4)	< 0.005 %
Barium (Ba)	< 0.01 %
Calcium (Ca)	0.01 %
Iron (Fe)	0.001 %
Lead (Pb)	< 0.0005 %
Potassium (K)	< 0.005 %
Silicon (Si)	0.002 %
Sodium (Na)	0.3 %
Cadmium	< 2.0 ppm

Table 6. Composition of syringe pump cylinder.

Component	Amount*
Carbon	0.06 % maximum
Manganese	4.0/6.0 %
Phosphorous	0.04 % maximum
Sulfur	0.03 % maximum
Silicon	1.0 % maximum
Chromium	20.5/23.5 %
Nickel	11.5/13.5 %
Molybdenum	1.5/3.0 %
Columbium	0.1/0.3 %
Vanadium	0.1/0.3 %
Nitrogen	0.2/0.4 %

*Note: Iron comprises the rest of the alloy.

graphite furnace atomic adsorption spectroscopy. We found approximately 0.8 ppb of chrome, 2.8 ppb of nickel, 19 ppb of iron, and 1.6 ppb of manganese present in the solution sampled from the pump. We suspect most of the nickel, chrome, and manganese were from minor dissolution of the pump cylinder alloy, perhaps aided by the preliminary acid-washing of the pump cylinder.

Electron microprobe energy dispersive analysis suggests that precipitation is a definite possibility. This evidence, when combined with the low effluent copper concentration and lack of evidence for significant participation of sodium in ion exchange, suggests that this experiment successfully precipitated copper minerals on the membrane from an initially 80% saturated copper carbonate solution.

Experiment WRRI4

This experiment hyperfiltrated an 80% saturated copper carbonate solution through a sedimented clay membrane. The final flow rate through the membrane was 100 ml/hour and the final ΔP was 4.9 bars (72 psi) (Table 7). The input alkalinity for this experiment was 0.177 mN and by the end of the experiment the alkalinity of the pump solution had risen to 0.201 mN, a 13.6% increase (Table 8). The analytical precision of the alkalinity titrations were $\pm$ 2% at two standard deviations. Therefore, there was a significant membrane effect for alkalinity. However, the copper concentration in the cell was slightly less than the copper concentration in the pump solution at the end of the experiment. This could be due to either precipitation or ion exchange, or might simply be an error in the data. As in experiment WRRI2, the copper concentration in the effluent was quite low for the experiment's duration. However, the effluent copper concentration did climb more significantly toward the end of experiment WRRI4 (Table 8) than in experiment WRRI2 (Table 4).

Scanning electron photomicrographs and electron microprobe energy dispersive analysis reveal particles on the membrane (Fig. 10) which contain only copper (Fig. 11) and no nickel. We suspect these particles may be copper carbonate. However, since carbon was used as the coating agent, confirmation of the presence of the carbonate phase is difficult. Unlike experiment WRRI2, no nickel, or iron is present in the particles we observed on the surface of the membrane. However, nickel and chrome concentrations in the pump solution and in the effluent are similar to those recorded in experiment WRRI2. The observed particles were common but not abundant. Typically, one to four particles were visible in an area of 100μm on a side. Some displayed a good crystallinity while others appeared to be amorphous (Fig. 11).

Table 7. Data for experiment WRRI4.

Sample No.	Date	Sample Interval (hours)	Total Elapsed Time (hours)	Sample Volume (cm^3)	Total Volume Collected (cm^3)	ΔP (bars)	pH
WRRI4-1	2-10-96	--	--	106.12	106.12	--	6.35
WRRI4-2	2-10-96	1.000	1.000	100.00	206.12	2.55	5.93
WRRI4-3	2-10-96	1.000	2.000	125.44	331.56	2.69	5.89
WRRI4-4	2-10-96	1.000	3.000	100.83	432.39	2.76	5.89
WRRI4-5	2-10-96	1.017	4.017	100.72	533.11	2.83	6.09
WRRI4-6	2-10-96	0.950	4.967	99.57	632.68	2.83	6.09
WRRI4-7	2-10-96	0.950	5.917	100.85	733.53	3.10	6.24
WRRI4-8	2-10-96	0.950	6.867	94.27	827.80	3.10	6.20
WRRI4-9	2-11-96	1.017	7.884	100.73	928.53	3.17	6.22
WRRI4-10	2-11-96	1.000	8.884	117.69	1046.22	3.24	5.96
WRRI4-11	2-11-96	0.950	9.834	97.57	1143.79	3.24	6.72
WRRI4-12	2-11-96	0.950	10.784	92.00	1235.79	3.24	7.10
WRRI4-13	2-11-96	4.333	15.117	436.4	1672.2	3.59	6.08
WRRI4-14	2-11-96	4.400	19.517	437.7	2109.9	3.72	6.53
WRRI4-15	2-11-96	4.617	24.134	458.5	2568.4	3.86	6.37
WRRI4-16	2-11-96	4.300	28.434	430.6	2999.0	4.14	6.33
WRRI4-17	2-12-96	4.533	32.967	456.4	3455.4	4.27	6.29
WRRI4-18	2-12-96	4.366	37.333	435.6	3891.0	4.41	6.32
WRRI4-19	2-12-96	4.433	41.766	444.6	4335.6	4.62	6.21
WRRI4-20	2-12-96	4.433	46.199	444.3	4779.9	4.62	6.05
WRRI4-21	2-12-96	4.600	50.799	461.2	5241.1	4.83	6.28
WRRI4-22	2-13-96	4.300	55.099	427.6	5668.7	4.90	6.36
WRRI4-23	2-13-96	3.600	58.699	360.6	6029.3	4.96	6.05
WRRI4-24	2-13-96	--	--	--	--	--	6.55
WRRI4-25	2-13-96	--	--	--	--	--	6.11
WRRI4-26	2-13-96	--	--	--	--	--	--

Table 8. Chemical analyses for experiment WRRI4.

	Chemical Analyses (performed by graphite furnace atomic absorption spectrometry unless otherwise noted)						
Sample No.	HCO_3 (mN)	Cu (ppb)	Cr (ppb)	Ni (ppb)	Na (ppb)	Ca (ppm)	Comments
WRRI4-1	0.177	169	0.6	2.4	858[1]	0[1]	Pump Solution
WRRI4-2	0.110	16.7	0.6	8.0	788[1]	0[1]	
WRRI4-3	0.135	8.9	1.3	0.9	782[1]	0[1]	
WRRI4-4	0.115	11.7	0.3	2.1	790[1]	0[1]	
WRRI4-5	0.101	9.1	0.7	1.2	846[1]	0[1]	
WRRI4-6	0.110	7.6	0.6	0.5	886[1]	0[1]	
WRRI4-7	0.159	7.6	0.5	1.8	968[1]	0[1]	
WRRI4-8	0.147	5.7	1.3	0.5	935[1]	0[1]	
WRRI4-9	0.135	7.6	0.5	0.9	959[1]	0[1]	
WRRI4-10	0.152	7.9	0.4	0.8	1051[1]	0[1]	
WRRI4-11	0.149	10.2	0.9	1.0	986[1]	0[1]	
WRRI4-12	0.151	17.8	0.8	0.9	962[1]	0[1]	
WRRI4-13	0.163	27.2	0.2	1.1	965[1]	0[1]	
WRRI4-14	0.154	9.4	0.2	0.9	969[1]	0[1]	
WRRI4-15	0.167	11.2	0.3	2.9	987[1]	0[1]	
WRRI4-16	0.168	19.0	0.5	4.5	1009[1]	0[1]	
WRRI4-17	0.177	14.0	0.4	1.8	9971	0[1]	
WRRI4-18	0.172	12.4	0.5	1.4	959[1]	0[1]	
WRRI4-19	0.172	32.9	0.2	0.8	915[1]	0[1]	
WRRI4-20	0.182	41.9	0.3	1.4	947[1]	0[1]	
WRRI4-21	0.190	52.2	1.2	1.2	941[1]	0[1]	
WRRI4-22	0.207	64.9	0.5	2.0	1135[1]	0[1]	
WRRI4-23	0.225	60.5	1.8	1.8	1053[1]	0[1]	
WRRI4-24	0.201	227	0.5	5.5	889[1]	0[1]	Pump Solution
WRRI4-25	0.245	179	0.3	2.8	1818[1]	0[1]	Cell Solution
WRRI4-26	--	1.6	0.3	1.2	0[1]	0[1]	Blank

[1]analyses by flame atomic absorption
[2]analyses by titration

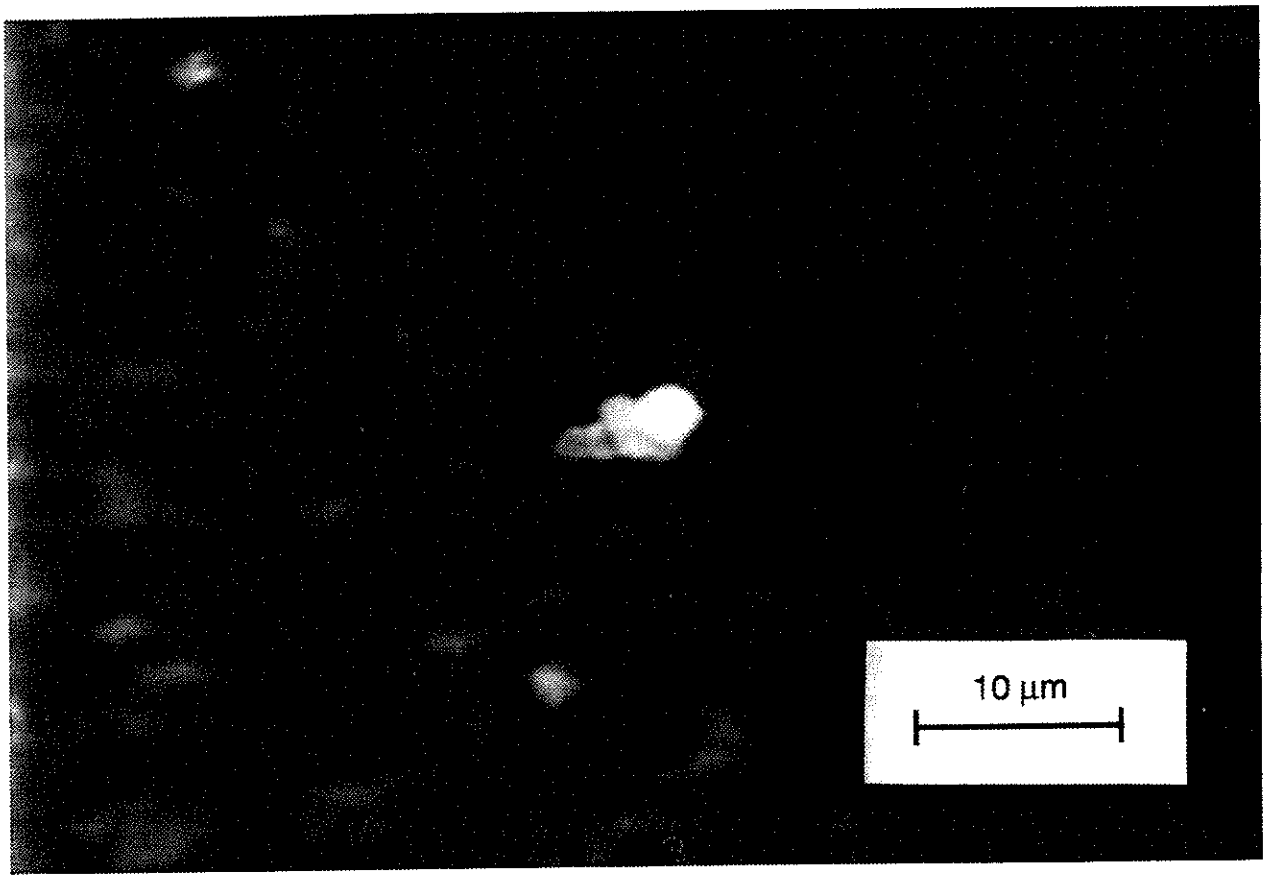

Figure 10. Scanning electron photomicrograph of copper particles on the surface of the sedimented clay membrane from experiment WRRI4.

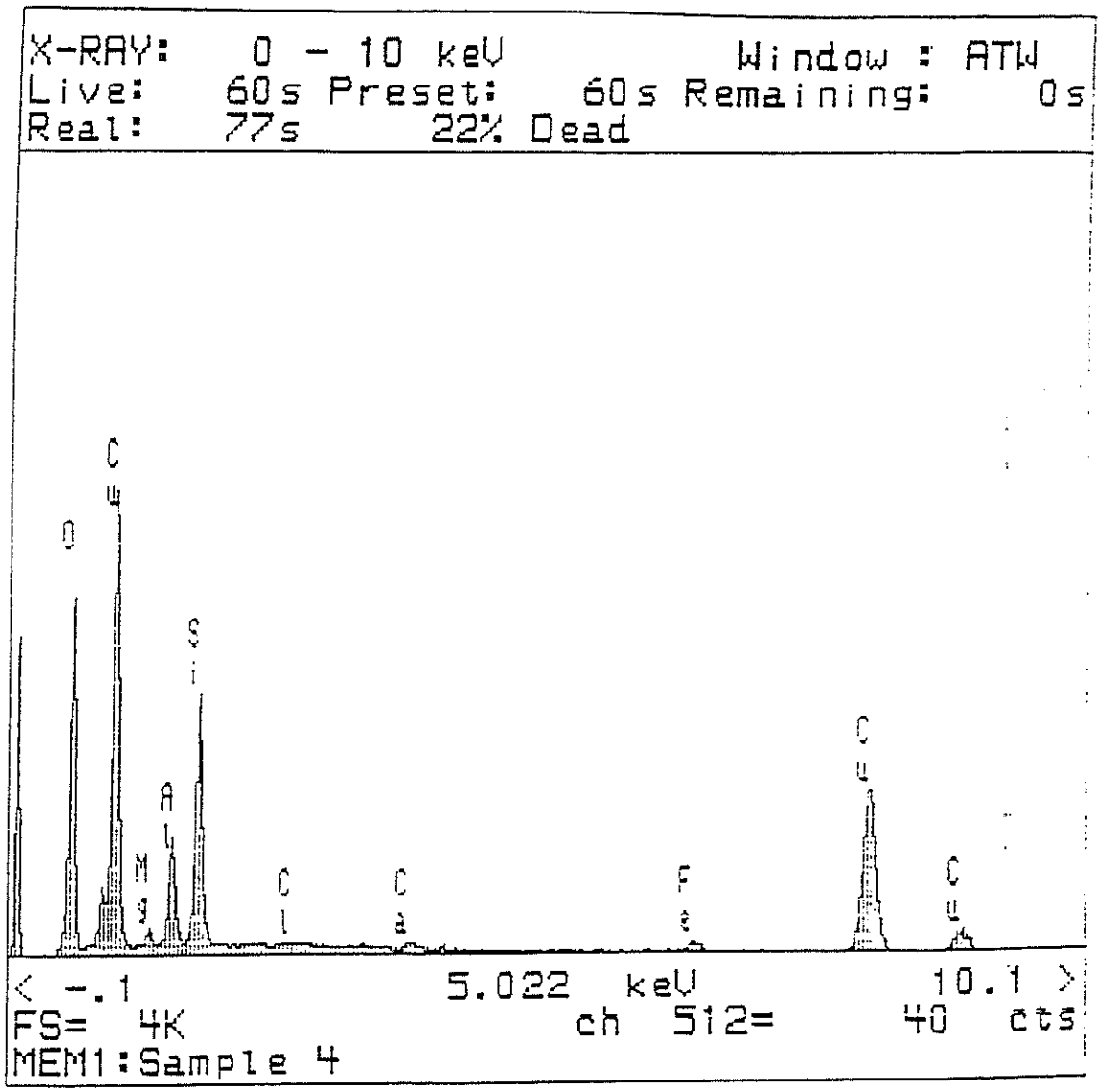

Figure 11. Energy dispersive spectra of elements present in particle on the surface of the sedimented clay membrane from experiment WRRI4.

Experiment WRRI7

This experiment hyperfiltrated an 80% saturated copper carbonate solution through a sedimented clay membrane at 10 ml/hour. The final ΔP for this experiment was 6.2 bars (91 psi) (Table 9). Both the alkalinity and copper concentration of the cell solution were lower than the alkalinity and copper concentrations in the input solution by 43% and 18 %, respectively. However, there was a significant decrease in bicarbonate alkalinity in the final aliquot sampled from the pump. The stock solution used in this experiment may have been poorly buffered and may have undergone interaction with atmospheric CO_2 in the storage container during the experiment. The copper concentration in the pump solution remained steady, however (Table 10). Significant Na (2.7 ppm) and Ca (4.4 ppm) were present in the make-up water used for this experiment due to a problem with the deionizer system. The Na concentration in the effluent began lower than the background Na concentration and slowly rose to slightly above background in the last half of effluent samples collected. This is probably the result of the exchange of copper and calcium cations for sodium cations attached to the clay membrane.

Scanning electron microscopy determined no particles were visible on the surface of the membrane. Electron microprobe element mapping failed to determine the presence of copper or nickel. The membrane was apparently barren of precipitate. This may be because steady-state C_o may have been less than solubility in this experiment or because steady-state was never reached.

Table 9. Data for experiment WRRI7.

Sample No.	Date	Sample Interval (hrs)	Elapsed Time (hrs)	Sample Vol. (cm^3)	Total Vol. Collected (cm^3)	ΔP (bars)	pH
WRRI7-1	4/14/96	--	--	--	--	--	7.28
WRRI7-2	4/14/96	6.60	6.60	89.02	89.02	8.16	4.33
WRRI7-3	4/15/96	8.32	14.92	81.73	170.75	8.37	4.83
WRRI7-4	4/15/96	7.68	22.60	77.02	247.77	8.57	5.11
WRRI7-5	4/15/96	11.92	34.52	119.68	367.45	8.57	5.43
WRRI7-6	4/16/96	12.05	46.57	118.67	486.12	4.15	5.71
WRRI7-7	4/16/96	11.75	58.32	118.57	604.69	5.17	5.95
WRRI7-8	4/17/96	11.83	70.15	116.71	721.40	5.31	5.52
WRRI7-9	4/17/96	12.42	82.57	123.26	844.66	5.37	3.97
WRRI7-10	4/18/96	12.05	94.62	120.68	965.34	5.92	6.09
WRRI7-11	4/18/96	11.63	106.25	115.94	1081.28	5.71	6.50
WRRI7-12	4/19/96	12.02	118.27	119.45	1200.73	5.92	6.70
WRRI7-13	4/19/96	12.10	130.37	120.52	1321.25	5.78	6.53
WRRI7-14	4/20/96	12.75	143.12	130.40	1451.65	6.12	6.94
WRRI7-15	4/20/96	11.93	155.05	115.68	1567.33	5.99	6.05
WRRI7-16	4/21/96	11.13	166.18	110.98	1678.31	6.19	5.63
WRRI7-17	4/21/96	--	--	--	--	--	7.06
WRRI7-18	4/21/96	--	--	--	--	--	5.76

Table 10. Chemical analyses for experiment WRRI7.

Sample No.	HCO_3 (mN)	Cu (ppb)	Cr (ppb)	Ni (ppb)	Na (ppb)	Ca (ppb)	Comments
WRRI7-1	0.394	125[1]	2.5	1.2	2730[1]	4360[1]	Pump Solution
WRRI7-2	0	3.2	5.3	4.9	859[1]	3790[1]	
WRRI7-3	0	3.5	3.3	2.6	1764[1]	2360[1]	
WRRI7-4	0	1.7	15.6	1.3	2340[1]	1300[1]	
WRRI7-5	0.046	2.3	9.9	0.9	2126[1]	404[1]	
WRRI7-6	0.083	1.5	2.4	0.8	2409[1]	73[1]	
WRRI7-7	0.071	1.4	16.6	4.1	2577[1]	129[1]	
WRRI7-8	0.071	2.7	4.6	1.2	2713[1]	129[1]	
WRRI7-9	0	2.4	6.9	0.9	2766[1]	104[1]	
WRRI7-10	0.109	2.7	1.0	0.4	2809[1]	85[1]	
WRRI7-11	0.135	3.7	0.3	0.8	2826[1]	91[1]	
WRRI7-12	0.141	6.8	0.9	0.7	2895[1]	79[1]	
WRRI7-13	0.098	5.8	0.4	0.6	2942[1]	104[1]	
WRRI7-14	0.098	5.9	0.3	0.7	2993[1]	104[1]	
WRRI7-15	0.095	7.6	0.4	0.6	3005[1]	104[1]	
WRRI7-16	0.048	8.6	0.8	1.6	3053[1]	91[1]	
WRRI7-17	0.078	124[1]	0.8	1.8	2890[1]	4619[1]	Pump Solution
WRRI7-18	0.044	102[1]	1.2	2.0	3172[1]	408[1]	Cell Solution

Chemical Analyses: (performed by graphite furnace atomic absorption spectrometry unless otherwise noted)
[1]analyses by flame atomic absorption
[2]analyses by titration

Experiment WRRI5

This experiment hyperfiltrated an 80% saturated solution of $PbCl_2$ through a sedimented clay membrane at 125 ml/hour. The final ΔP was 24.1 bars (355 psi) (Table 11). Chloride concentrations in the effluent remained consistently below the input chloride concentration. The chloride concentration in the pump remained consistent throughout the experiment (Table 12). The chloride anion is conservative and does not significantly participate in ion exchange. Therefore, the decrease in Cl concentration in the effluent minus any concentration increase in the CPL is the result of precipitation at the membrane. However, this quantity is difficult to calculate for this experiment because the cell solution showed no increase in chloride concentration. This is likely due to the fact that the length of the CPL was very short in this experiment (CPL length is approximately equal to $10D/J_v$ which for this experiment = 0.08 cm). Thus it is difficult to collect a representative cell solution without disturbing the sedimented clay membrane at the end of the experiment.

The measured Pb concentrations are erratic (Table 12) and do not appear reliable because they suggest more lead exited the experimental cell than was input. This is impossible. We have no explaination for this other than possible error in the lead analyses.

A greenish-yellow precipitate was visible on the surface of the membrane through the clear acrylic experimental cell after about 12 hours. The experiment was stopped after 22.85 hours. Scanning electron photomicrographs of the membrane reveal the presence of numerous dendritic crystalline growths and particles (Fig. 12) present on its surface. Dendritic crystals are characteristic of rapid crystal growth. Electron microprobe energy dispersive analysis (Fig. 13) and X-ray fluorescence analysis reveal that these particles are comprised of lead chloride. X-ray analysis performed by the X-ray facility at the NMBMMR suggests that the mineral phase is cotunnite ($PbCl_2$).

Table 11. Data for experiment WRRI5.

Sample No.	Date	Sample Interval (hours)	Elapsed Time (hours)	Sample Volume (cm^3)	Total Volume Collected (cm^3)	ΔP (bars)	pH
WRRI5-1	3-12-96	--	--	--	--	--	3.01
WRRI5-2	3-12-96	0.917	0.917	112.53	112.53	19.03	2.94
WRRI5-3	3-12-96	1.000	1.917	124.90	237.43	19.44	2.96
WRRI5-4	3-12-96	1.000	2.917	122.66	360.09	19.79	3.00
WRRI5-5	3-12-96	0.917	3.834	121.33	481.42	20.06	2.97
WRRI5-6	3-12-96	1.000	4.834	129.97	611.39	21.51	2.98
WRRI5-7	3-12-96	1.000	5.834	126.31	737.70	21.37	2.96
WRRI5-8	3-12-96	1.000	6.834	128.49	866.19	22.20	2.98
WRRI5-9	3-13-96	1.000	7.834	120.63	986.82	22.27	2.95
WRRI5-10	3-13-96	0.933	8.767	123.62	1110.44	25.23	2.91
WRRI5-11	3-13-96	0.983	9.750	126.17	1236.61	25.51	2.99
WRRI5-12	3-13-96	1.033	10.783	126.53	1363.14	25.65	2.99
WRRI5-13	3-13-96	0.933	11.716	117.82	1480.96	25.72	3.09
WRRI5-14	3-13-96	0.900	12.616	117.93	1598.89	24.48	2.97
WRRI5-15	3-13-96	0.883	13.499	111.16	1710.05	24.55	3.00
WRRI5-16	3-13-96	0.883	14.382	111.44	1821.49	24.68	2.97
WRRI5-17	3-13-96	0.967	15.349	120.10	1941.59	24.68	3.04
WRRI5-18	3-13-96	0.850	16.199	109.18	2050.77	24.61	3.00
WRRI5-19	3-13-96	0.917	17.116	115.23	2166.00	24.75	2.99
WRRI5-20	3-13-96	0.933	18.049	118.11	2284.11	24.82	2.99
WRRI5-21	3-13-96	0.917	18.966	112.97	2397.08	24.82	2.97
WRRI5-22	3-13-96	0.917	19.883	118.35	2515.43	24.68	2.97
WRRI5-23	3-13-96	1.067	20.950	133.08	2648.51	24.68	3.02
WRRI5-24	3-13-96	0.933	21.883	118.80	2767.31	24.55	3.02
WRRI5-25	3-13-96	0.967	22.850	123.11	2890.42	24.48	2.97
WRRI5-26	3-13-96	--	--	--	--	--	--
WRRI5-27	3-13-96	--	--	--	--	--	3.04

Table 12. Chemical analyses for experiment WRRI5.

Sample No.	Cl (ppm)	Pb (ppm)	Na (ppm)	Ca (ppm)	Comments
WRRI5-1	1931	4561	0	0	pump solution
WRRI5-2	1844	4159	0	15.7	
WRRI5-3	1901	4908	0	0	
WRRI5-4	1896	5897	0	0	
WRRI5-5	1852	5834	0	0	
WRRI5-6	1832	6012	0	0	
WRRI5-7	1965	5639	0	0	
WRRI5-8	1898	5769	0	0	
WRRI5-9	1944	5611	0	0	
WRRI5-10	1894	5686	0	0	
WRRI5-11	1873	5632	0	0	
WRRI5-12	1851	5583	0	0	
WRRI5-13	1840	5436	0	0	
WRRI5-14	1880	5901	0	0	
WRRI5-15	1871	5564	0	0	
WRRI5-16	1916	6181	0	0	
WRRI5-17	1716	5615	0	0	
WRRI5-18	1922	5679	0	0	
WRRI5-19	1889	4844	0	0	
WRRI5-20	1785	5334	0	0	
WRRI5-21	1807	5271	0	0	
WRRI5-22	1778	5072	0	0	
WRRI5-23	1777	4819	0	0	
WRRI5-24	1819	4778	0	0	
WRRI5-25	1837	5597	0	0	
WRRI5-26	1900	4883	0	0	cell solution
WRRI5-27	1927	4987	0	0	pump solution

Note: Chloride analyses performed by titration, Pb, Na, and Ca analyses performed by flame atomic absorption.

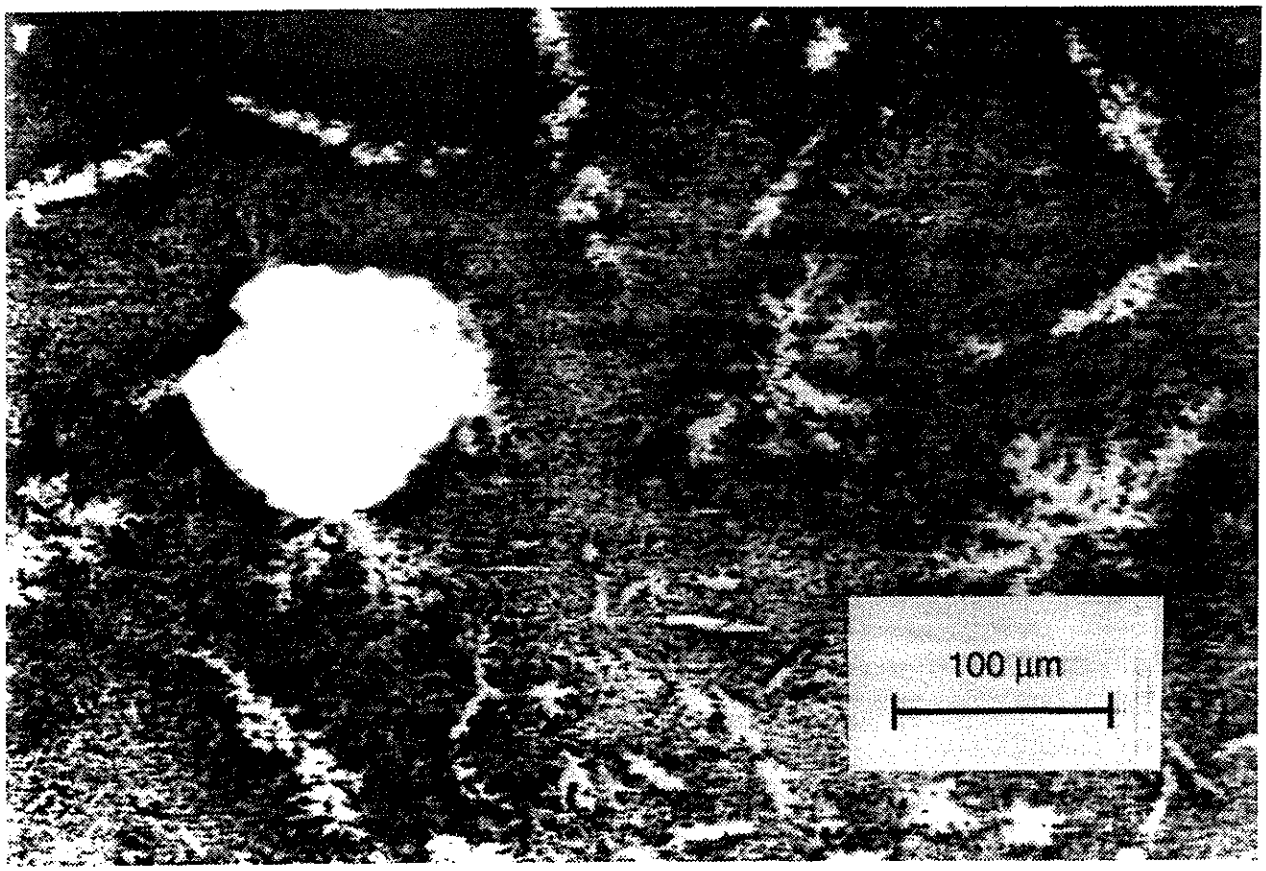

Figure 12. Scanning electron photomicrograph of lead chloride particle on the surface of the sedimented clay membrane from experiment WRRI5.

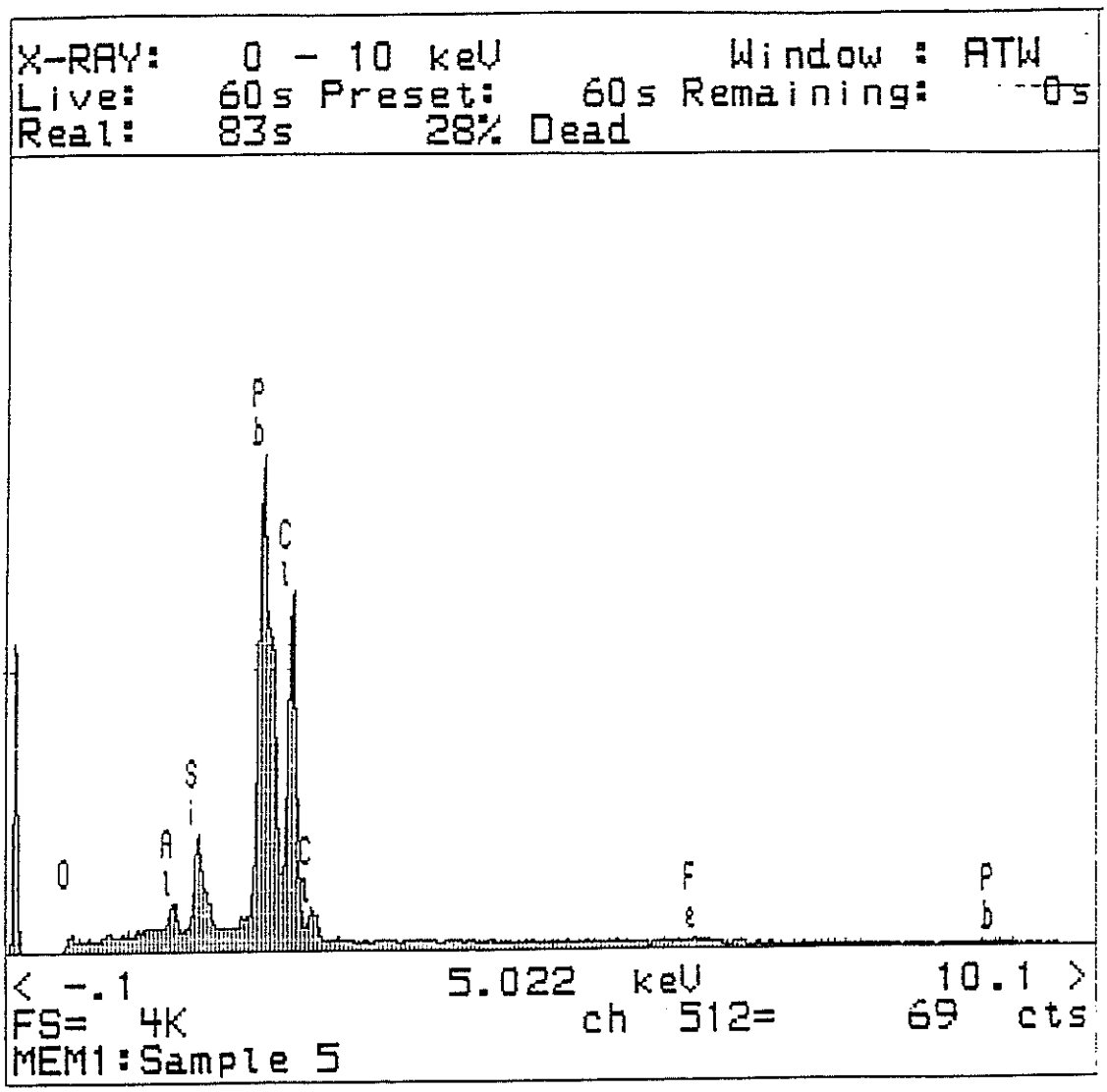

Figure 13. Energy dispersive spectra of elements present in particle on the surface of the sedimented clay membrane from experiment WRRI5. Further X-ray diffraction analysis performed at the NMBMMR X-ray facility shows that the precipitate is cotunnite ($PbCl_2$).

Experiment WRRI6

This experiment hyperfiltrated a 23% saturated lead chloride solution through a sedimented clay membrane at 75 ml/hour. The final ΔP was 16.4 bars (241 psi) (Table 13). The effluent chloride concentration dropped slightly in the first aliquot and then rose in subsequent aliquots (Table 14) until it quickly approached the input concentration. The lead analyses again tended to suggest that slightly more lead exited the experimental cell than entered it. Again, this is impossible and we suspect a problem with the analysis. No calcium was detected in the effluent, however, some 40.6 ppm of Na was present in the first effluent sample suggesting a significant amount of ion exchange occurred early in the experiment. The Na concentration in the effluent quickly dropped until by the eighth effluent sample, no Na was detectable.

A greenish-yellow precipitate was visible on the surface of the membrane through the clear acrylic experimental cell when the experiment was stopped after 25.28 hours. Scanning electron photomicrographs reveal numerous, dendritic crystal masses on the surface of the membrane (Fig. 14) and electron microprobe energy dispersive analysis reveals that these crystals are composed of lead chloride (Fig. 15).

Table 13. Data for experiment WRRI6.

Sample No.	Date	Sample Interval (hours)	Elapsed Time (hours)	Sample Volume (cm^3)	Total Volume Collected (cm^3)	ΔP (bars)	pH
WRRI6-1	3-17-96	--	--	--	--	--	4.17
WRRI6-2	3-17-96	0.850	0.850	66.13	66.13	16.27	3.92
WRRI6-3	3-17-96	1.167	2.017	87.69	153.82	16.20	4.00
WRRI6-4	3-17-96	1.300	3.317	97.65	251.47	16.24	4.10
WRRI6-5	3-17-96	1.250	4.567	93.59	345.06	16.13	4.10
WRRI6-6	3-17-96	1.200	5.767	89.87	434.93	16.06	4.13
WRRI6-7	3-17-96	1.350	7.117	102.49	537.42	15.65	4.15
WRRI6-8	3-17-96	1.600	8.717	120.33	657.75	15.79	4.20
WRRI6-9	3-17-96	1.733	10.450	129.79	787.54	16.00	4.20
WRRI6-10	3-18-96	1.733	12.183	130.12	917.66	16.10	4.14
WRRI6-11	3-18-96	1.767	13.950	134.59	1052.25	16.20	4.19
WRRI6-12	3-18-96	1.733	15.683	128.85	923.40	16.41	4.18
WRRI6-13	3-18-96	1.367	17.050	102.41	820.99	16.48	4.22
WRRI6-14	3-18-96	1.683	18.733	125.94	946.93	16.48	4.22
WRRI6-15	3-18-96	1.583	20.316	121.96	1068.89	16.69	4.20
WRRI6-16	3-18-96	1.867	22.183	138.48	1207.37	16.75	4.28
WRRI6-17	3-18-96	1.417	23.600	105.77	1313.14	16.55	4.27
WRRI6-18	3-18-96	1.683	25.283	125.79	1438.93	16.62	4.28
WRRI6-19	3-18-96	--	--	--	--	--	4.23
WRRI6-20	3-18-96	--	--	--	--	--	4.22

Table 14. Chemical analyses for experiment WRRI6.

Sample No.	Cl (ppm)	Pb (ppm)	Na (ppm)	Ca (ppm)	Comments
WRRI6-1	556	1569	0	0	Pump Solution
WRRI6-2	525	1393	40.6	0	
WRRI6-3	560	1532	0.82	0	
WRRI6-4	557	1497	0.23	0	
WRRI6-5	551	1601	0.29	0	
WRRI6-6	550	1660	0.28	0	
WRRI6-7	553	1493	0.17	0	
WRRI6-8	551	1601	0.05	0	
WRRI6-9	550	1605	0	0	
WRRI6-10	551	1662	0	0	
WRRI6-11	545	1719	0	0	
WRRI6-12	558	1652	0	0	
WRRI6-13	560	1627	0	0	
WRRI6-14	561	1556	0	0	
WRRI6-15	560	1595	0	0	
WRRI6-16	553	1612	0	0	
WRRI6-17	553	1811	0	0	
WRRI6-18	553	1679	0	0	
WRRI6-19	550	1487	0	0	Pump Solution
WRRI6-20	577	1696	0	0	Cell Solution

Note: Chloride analyses performed by titration, Pb, Na, and Ca analyses performed by flame atomic absorption.

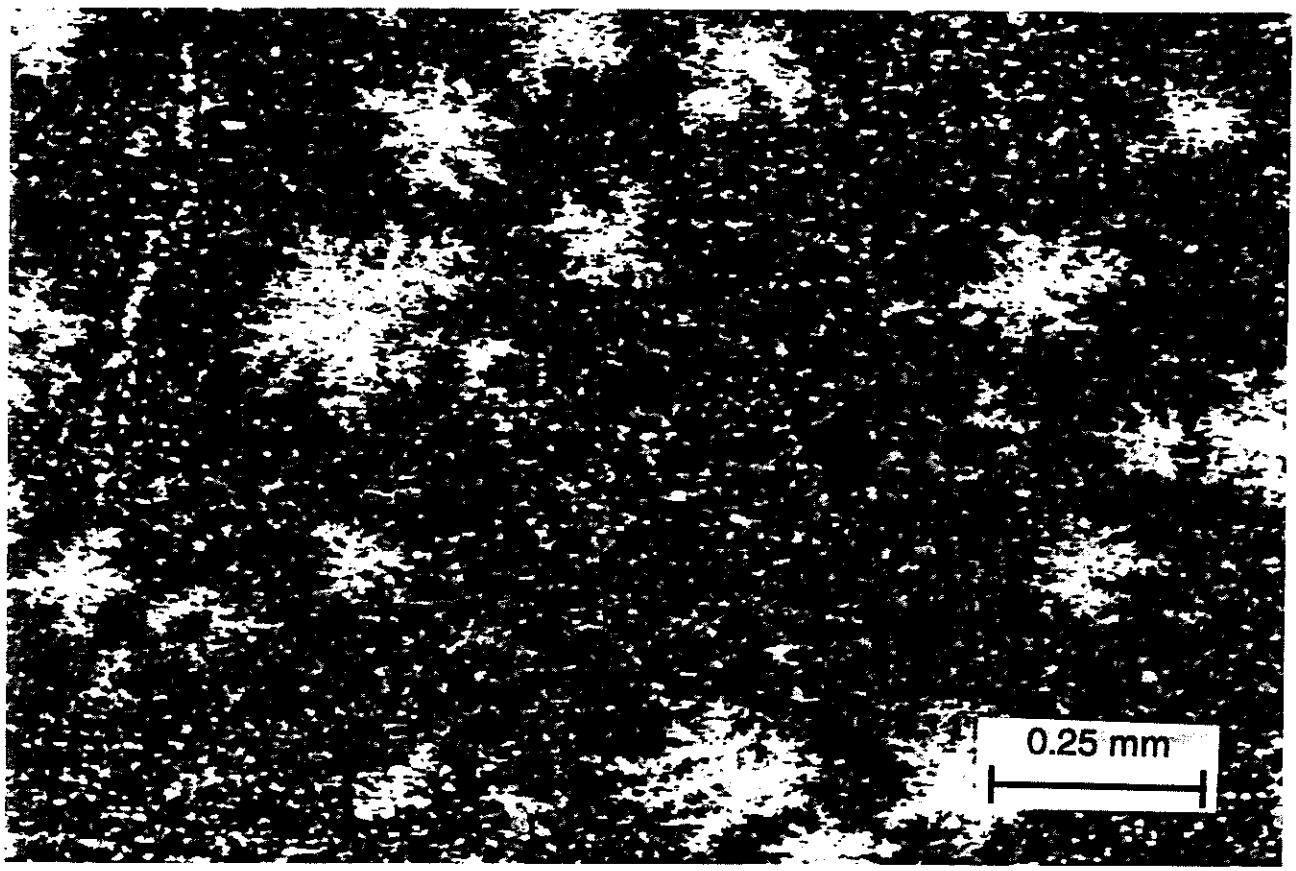

Figure 14. Scanning electron photomicrograph of lead chloride particles on the surface of the sedimented clay membrane from experiment WRRI6.

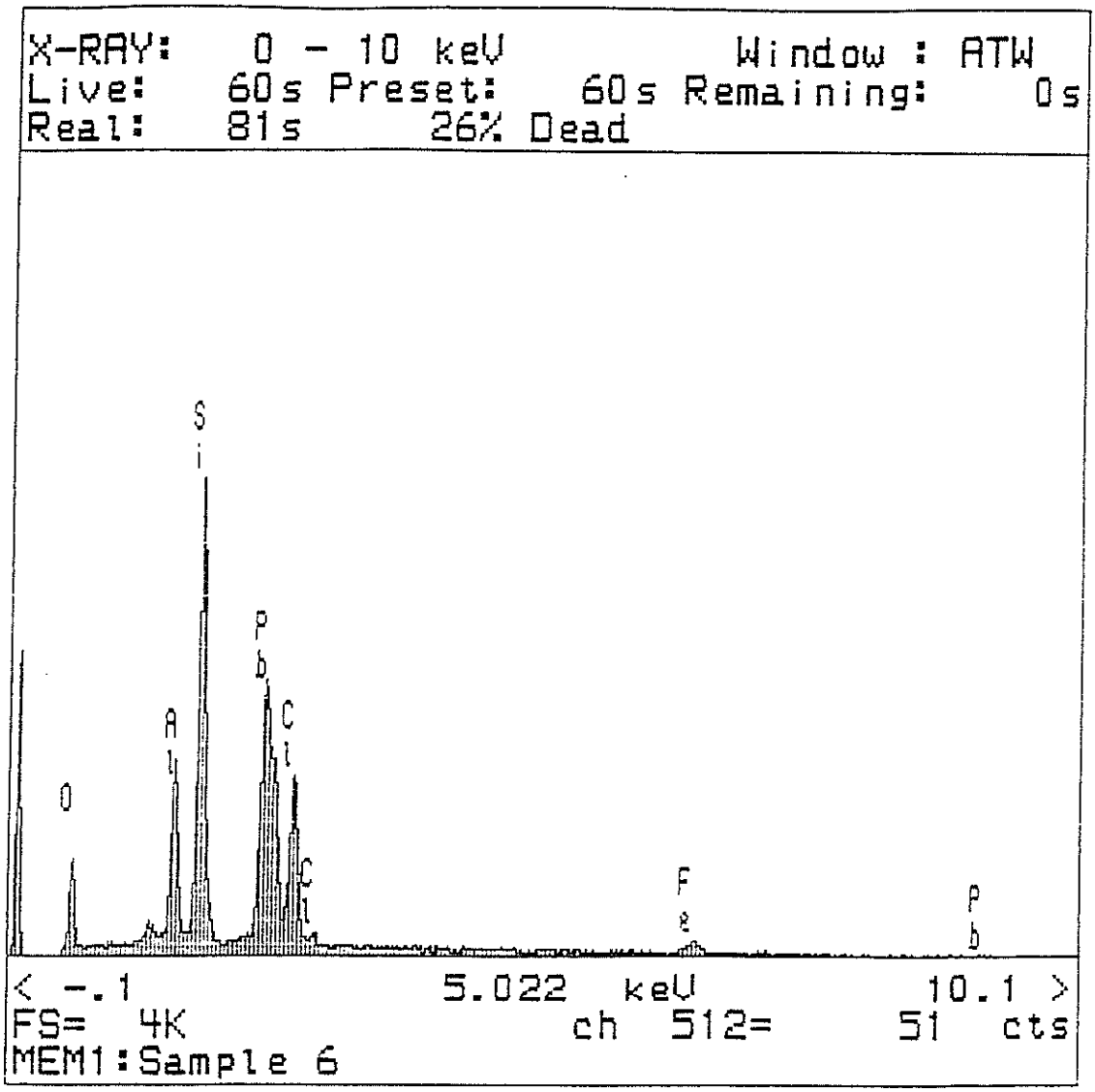

Figure 15. Energy dispersive spectra of elements present in particle on the surface of the sedimented clay membrane from experiment WRRI6.

Experiment WRRI8

Experiment WRRI-8 hyperfiltrated an 80% saturated $CuCl_2$ solution through a sedimented clay membrane at 150 ml/hr. The final ΔP was 66.3 bars (975 psi) (Table 15). At ten hours into the experiment, a greenish-yellow precipitate was observed on the membrane. After the cell solution was decanted, the membrane was repeatedly washed with ethanol and then saved for examination. Chemical analyses for this experiment are reported in Table 16.

Figure 16 is a scanning electromicrograph pf the precipitate on the membrane. Figure 17 is a graph of energy dispersive spectra of elements present in particle on the surface of the sedimented clay membrane showing the particles to be copper chloride.

Table 15. Data for experiment WRRI8.

Sample No.	Date	Sample Interval (hours)	Elapsed Time (hours)	Sample Volume (cm^3)	Total Volume Collected (cm^3)	ΔP (bars)	pH
WRRI8-1	8-18-96		--	--	--	--	3.83
WRRI8-2	8-18-96	0.50	0.50	67.48	67.48	279	3.19
WRRI8-3	8-18-96	0.52	1.02	78.38	145.86	312	3.22
WRRI8-4	8-18-96	0.83	1.85	138.66	284.52	355	3.27
WRRI8-5	8-18-96	0.83	2.68	106.97	391.49	397	3.18
WRRI8-6	8-18-96	0.72	3.40	109.52	501.01	444	3.15
WRRI8-7	8-18-96	0.80	4.20	122.01	379.00	472	3.27
WRRI8-8	8-18-96	0.80	5.00	125.17	504.17	499	3.18
WRRI8-9	8-18-96	1.00	6.00	152.85	657.02	509	3.18
WRRI8-10	8-18-96	1.18	7.18	170.69	827.71	560	3.25
WRRI8-11	8-18-96	1.07	8.25	170.88	998.59	589	3.17
WRRI8-12	8-18-96	1.63	9.88	244.09	1242.68	675	3.10
WRRI8-13	8-19-96	1.52	11.40	230.71	1473.39	713	3.17
WRRI8-14	8-19-96	2.57	13.97	380.72	1854.11	825	3.12
WRRI8-15	8-19-96	2.80	16.77	426.98	2281.09	923	3.10
WRRI8-16	8-19-96	1.40	18.77	220.96	2502.05	975	3.14
WRRI8-17	8-19-96	--	--	--	--	--	3.08
WRRI8-18	8-19-96	--	--	--	--	--	3.15

Table 16. Chemical analyses for experiment WRRI8.

Sample No.	Cl (ppm)	Cu (ppm)	Comments
WRRI8-1	2309	1881	Pump solution
WRRI8-2	1978	695	
WRRI8-3	1999	1762	
WRRI8-4	2194	1842	
WRRI8-5	2151	1825	
WRRI8-6	2203	1756	
WRRI8-7	2160	1768	
WRRI8-8	2163	1787	
WRRI8-9	1975	1704	
WRRI8-10	2242	1728	
WRRI8-11	1918	1666	
WRRI8-12	2202	1815	
WRRI8-13	1818	1833	
WRRI8-14	2244	1823	
WRRI8-15	2257	1859	
WRRI8-16	2271	1850	
WRRI8-17	2040	1953	Cell Solution
WRRI8-18	2195	1842	Pump Solution

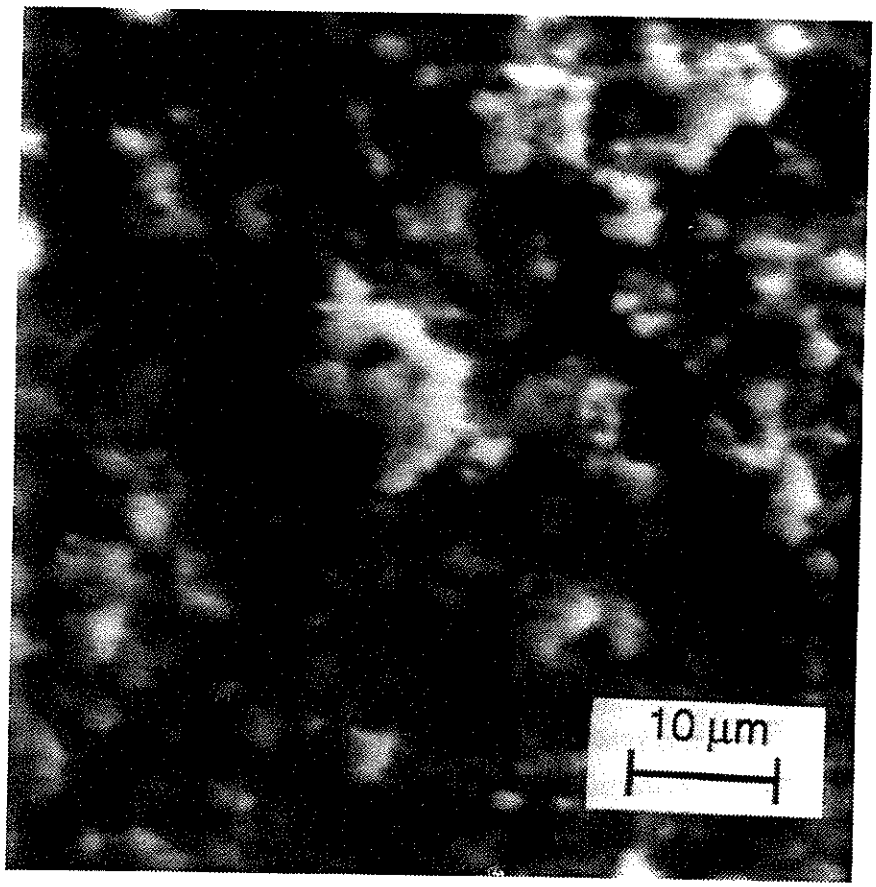

Figure 16. Scanning electron photomicrograph of copper chloride particles on the surface of the sedimented clay membrane from experiment WRRI8.

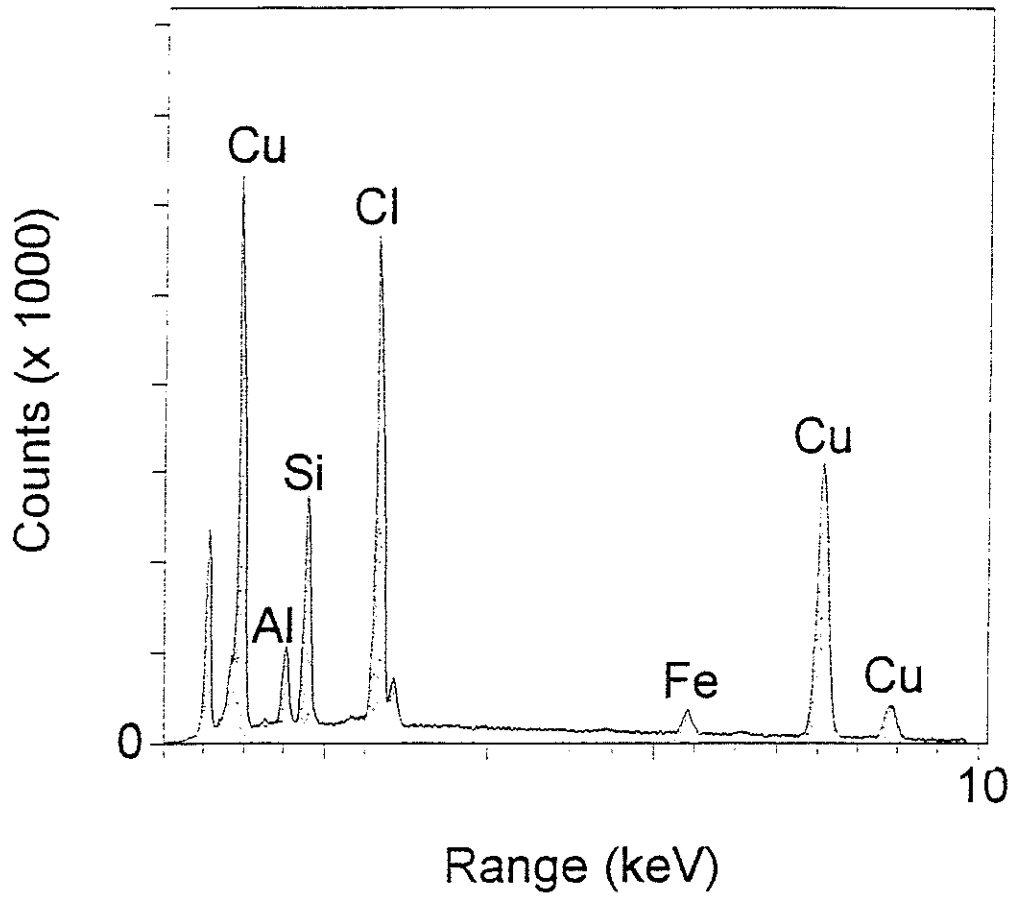

Figure 17. Energy dispersive spectra of elements present in particle on the surface of the sedimented clay membrane from experiment WRRI8.

Experiment WRRI9

Experiment WRRI-9 hyperfiltrated an 80% saturated $CoCl_2$ solution through a sedimented clay membrane at 100 ml/hr. The final ΔP was 63 bars (926 psi) (Table 17). Due to the strong reddish color of the solution, it was difficult to tell if a precipitate was forming during the experiment. However, when the cell was disassembled, a small amount of reddish precipitate was visible on the surface of the membrane. After the cell solution was decanted, the membrane was washed repeatedly in ethanol, and stored for later examination.

Table 17. Data for experiment WRRI9.

Sample No.	Date	Sample Interval (hours)	Elapsed Time (hours)	Sample Volume (cm^3)	Total Volume Collected (cm^3)	ΔP (bars)	pH
WRRI9-1	9-23-96	--	--	--	--	--	3.95
WRRI9-2	9-23-96	0.70	0.70	67.40	67.40	16.60	4.42
WRRI9-3	9-23-96	0.90	1.60	93.55	160.95	21.56	4.38
WRRI9-4	9-23-96	0.87	2.47	85.33	246.28	25.92	4.19
WRRI9-5	9-23-96	1.05	3.52	104.86	351.14	28.44	4.26
WRRI9-6	9-23-96	1.15	4.67	114.18	465.32	31.90	4.32
WRRI9-7	9-23-96	1.45	6.12	146.53	611.85	37.76	4.31
WRRI9-8	9-23-96	1.72	7.83	173.17	785.02	41.36	4.23
WRRI9-9	9-24-96	2.15	9.98	218.57	1003.59	47.28	4.32
WRRI9-10	9-24-96	2.25	12.23	224.71	1228.30	50.75	4.29
WRRI9-11	9-24-96	2.13	14.37	218.60	1446.90	54.90	4.27
WRRI9-12	9-24-96	2.15	16.52	215.02	1661.92	56.87	4.26
WRRI9-13	9-24-96	2.07	18.58	206.82	1868.74	56.39	4.24
WRRI9-14	9-24-96	2.10	20.68	211.12	2079.86	58.84	4.25
WRRI9-15	9-24-96	2.03	22.72	207.44	2287.30	61.09	4.23
WRRI9-16	9-24-96	2.25	24.97	226.24	2513.54	62.99	4.25
WRRI9-17	9-24-96	--	--	--	--	--	4.01
WRRI9-18	9-24-96	--	--	--	--	--	4.28

Figure 18 is a scanning electromicrograph of the precipitate on the membrane. Figure 19 is a graph of energy dispersive spectra of elements present in particle on the surface of the sedimented clay membrane showing the particles to be cobalt chloride.

Table 18. Chemical analyses for experiment WRRI9.

Sample No.	Cl (ppm)	Co (ppm)	Comments
WRRI9-1	3028.	4.529	Pump solution
WRRI9-2	3,048	3.562	
WRRI9-3	3.119	3.897	
WRRI9-4	3,160	3.911	
WRRI9-5	3.245	3.986	
WRRI9-6	3,188	3.192	
WRRI9-7	3,074	4.138	
WRRI9-8	3.267	3.787	
WRRI9-9	3.117	3.263	
WRRI9-10	3.381	3.535	
WRRI9-11	3.658	3.352	
WRRI9-12	3.684	3.473	
WRRI9-13	2.684	3.096	
WRRI9-14	3,090	3.109	
WRRI9-15	3,238	3.143	
WRRI9-16	4.133	3.198	
WRRI9-17	4.167	3.319	Pump Solution
WRRI9-18	6.450	4.526	Cell Solution

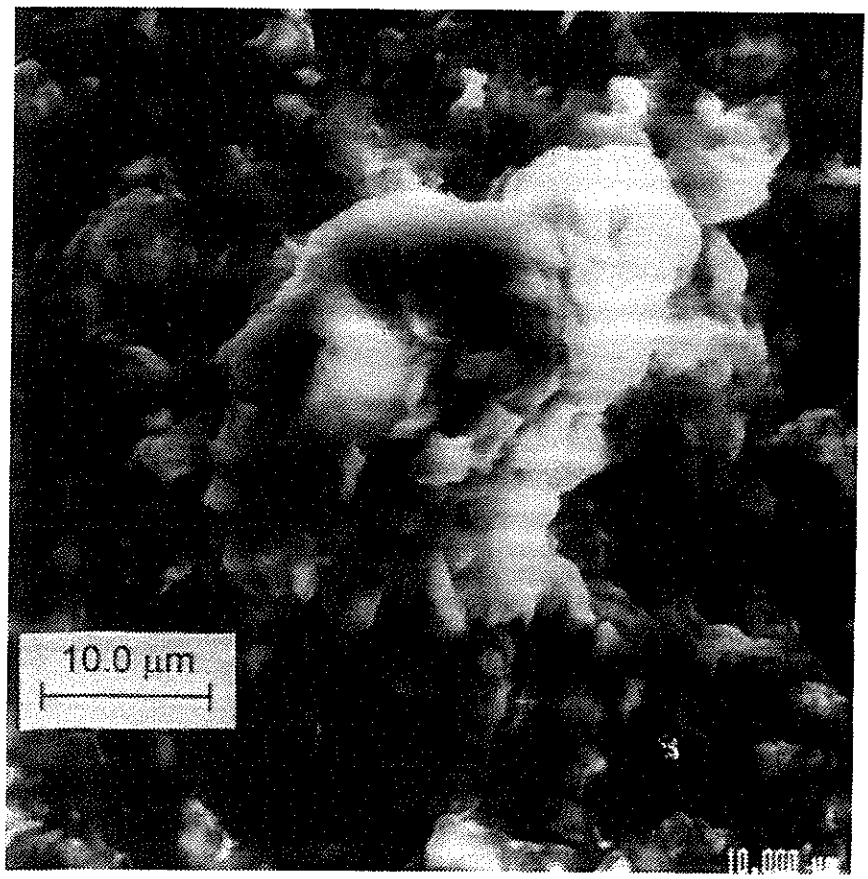

Figure 18. Scanning electron photomicrograph of cobalt chloride particles on the surface of the sedimented clay membrane from experiment WRRI9.

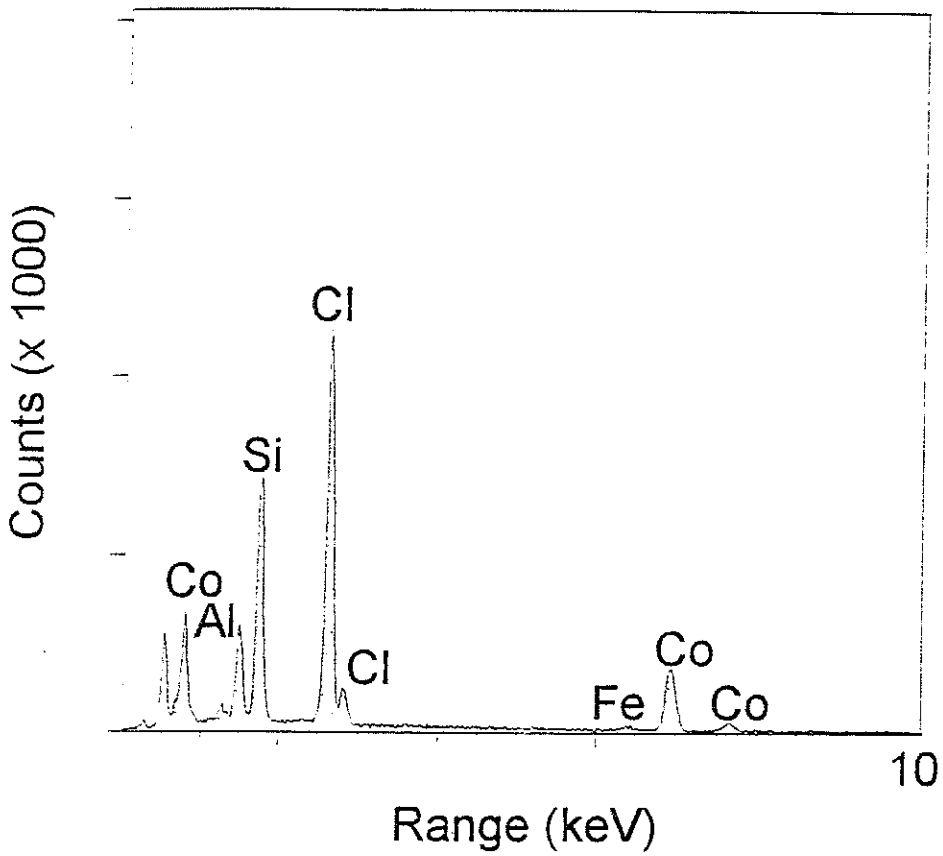

Figure 19. Energy dispersive spectra of elements present in particle on the surface of the sedimented clay membrane from experiment WRRI9.

Litho-Osmometer Experiments

The experiments with the first litho-osmometer design (Fig. 5) were not successful due to entrained air in the apparatus. However, the current run, which has not yet reached steady-state, suggests that time periods of more than four months may be necessary with some shales. Work is continuing on these experiments. However, it appears that this design is unsuitable for use in rapid determination of membrane coefficients. Therefore, a litho-osmometer on a different design (Fig. 6) was constructed. This design promises faster, although still rather long, operation times.

Before beginning the experiments, the entire system was tested for pressure leaks. Two steel disks were placed into the litho-osmometer so that it could be pressure tested. The pressure-testing process took two weeks and was deemed successful when the system pressure held for a period of three days.

We then performed the first test with a clayey siltstone (Fig. 20) using a 69.5 mM NaCl solution. The theoretical osmotic pressure for this solution is 49.98 psi. Note that the pressure decayed rapidly from 51 psi to about four psi. The pressure curve then went asymptotic to the x-axis at about 2.0 psi. When the pressure was set to zero and allowed to rise, it rose to 2 psi. This pressure needs to have a positive correction of 1.3 psi added due to the position of the transducer above the experimental cell. If 3.3 psi is assumed to be the equilibrium pressure, then $\sigma = 3.3/51 = 0.06$. This value is reasonable for a clayey siltstone. However, since the accuracy of the pressure transducer is $\pm$ 1.0 psi, σ could range from 0.08 to 0.05.

Because the pressure readings with the siltstone were in a range that is tenuous for the pressure transducer, we tried a run with a dark marine shale. This shale came from a core taken at 1602-1604 feet in the Tenneco Hospah #65 well, South Hospah Field, McKinley Co., NM ()NMBMMR core #1150, box 24) and is quite tight. Our first test used a 69.5 mM NaCl solution and ran for 72 hours (Fig. 21). The exponential decay equation

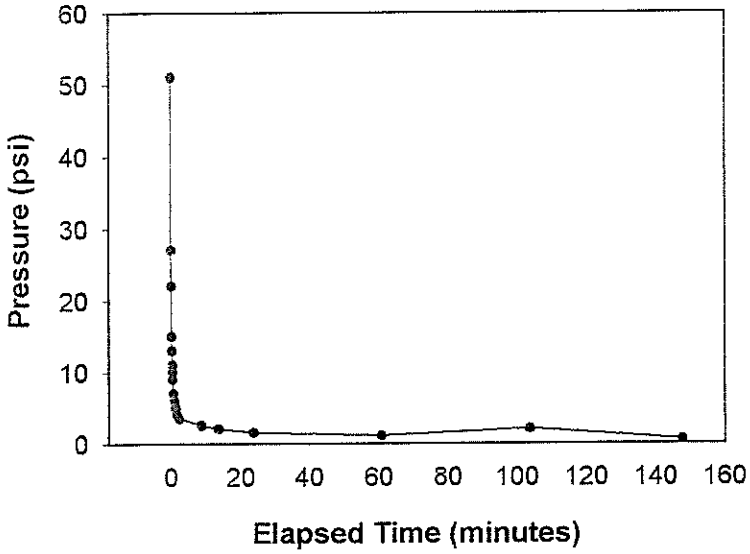

Figure 20. Plot of pressure decay data for siltstone.

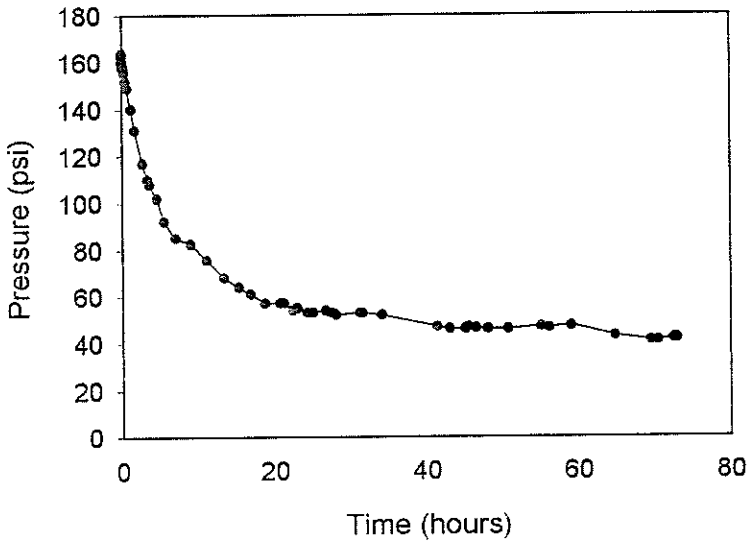

Figure 21. Plot of pressure decay data for shale.

$$\Delta P = 47.87 + 111.74EXP(-T/6.794) \quad (10)$$

where T is time in hours, was fit to the experimental data. The square of the regression coefficient was 0.9923. This equation becomes asymptotic to the x-axis at a pressure value of 47.9 psi. If actual equilibrium was at 47.9 psi, then $\sigma = 47.87/49.98 = 0.96$. A value for the reflection coefficient of 0.96 seems high but may indeed prove to be feasible for well-compacted, tight shales such as this one. However, the last few data points fell below the predicted equilibrium point suggesting that 47.87 psi may not be the true equilibrium point.

We next tried setting the pressure lower than the equilibrium point and waiting for it to rise toward equilibrium. We set the pressure to 15 psi and locked off the system. The pressure fell to 15 psi, then rose to 17 psi, and then fell again to 13 psi. We set the pressure at 20 psi for three more trys but each time it fell instead of rising. This suggests that 1) the theoretical equilibrium pressure value of 47.9 psi may not be correct, 2) there was air entrained in the system, or, 3) there was a leak in the system. We will continue research on this procedure. Our preliminary conclusion is that more work is necessary before evaluation of this method's potential is complete.

Calculation of Membrane Coefficients

Because mineral precipitation at the membrane and ion exchange within the membrane are obviously significant possibilities during the experiments performed for this study, it would be erroneous to use measured effluent concentrations to calculate steady-state values of σ. Therefore, it is necessary to derive a steady-state solution for σ that does not use the measured values for c_e. This can be done, because at steady-state $c_e = c_i$. Therefore, by substituting Equation 4 into Equation 1 we obtain

$$J_v = L_p(\Delta P - \sigma vRT(c_o - c_e) \quad (11)$$

which since $c_e = c_i$ at steady-state is the equivalent of

$$J_v = L_p(\Delta P - \sigma vRT(c_o - c_i) \quad (12)$$

Fritz and Marine (1983) stated that

$$\omega = \frac{D}{RT\Delta x\zeta} \tag{13}$$

where ζ is the tortuosity of the flow path through the membrane defined by the ratio of the actual length divided by the membrane thickness. By substituting Equation 4, Equation 13, and the steady-state relationship $J_S = J_v c_e$ into Equation 2 we obtain

$$J_v \cdot c_i = \frac{c_o + c_i}{2}(1-\sigma)J_v + \frac{D}{RT\Delta x\zeta} vRT(c_o - c_i) \tag{14}$$

Solving equations 12 and 14 for σ and setting them equal we obtain

$$\frac{L_p\Delta P - J_v}{L_p vRT(c_o - c_i)} = \frac{\frac{2Dv(c_o - c_i)}{\Delta x\zeta} - J_v(c_i - c_o)}{J_v(c_0 + c_i)} \tag{15}$$

Solving this equation for c_i yields a polynomial solution with two roots, one positive and one negative root.

$$\begin{aligned} root1 = {} & \frac{1}{2L_p vRT(J_v\Delta x - 2vD)} \cdot (-2L_p vRTJ_v c_i\Delta x\zeta - 4L_p v^2 RTDc_i + \Delta x\zeta J_v L_p\Delta P + \\ & \Delta x^{1/2}\zeta^{1/2}(-8\zeta\Delta x c_i J_v{}^3 TRvL_p + 8\zeta\Delta x c_i J_v{}^2 TRvL_p{}^2 + \zeta\Delta x J_v{}^4 - 2\zeta\Delta x\Delta P L_p J_v{}^3 + \\ & \zeta\Delta x\Delta P^2 L_p{}^2 J_v{}^2 - 16J_v{}^2 c_i DTRv^2 L_p{}^2)^{1/2} \end{aligned} \tag{16}$$

$$\begin{aligned} root2 = {} & \frac{1}{2L_p vRT(J_v\Delta x - 2vD)} \cdot (-2L_p vRTJ_v c_i\Delta x\zeta - 4L_p v^2 RTDc_i + \Delta x\zeta J_v L_p\Delta P - \\ & \Delta x^{1/2}\zeta^{1/2}(-8\zeta\Delta x c_i J_v{}^3 TRvL_p + 8\zeta\Delta x c_i J_v{}^2 TRvL_p{}^2 + \zeta\Delta x J_v{}^4 - 2\zeta\Delta x\Delta P L_p J_v{}^3 + \\ & \zeta\Delta x\Delta P^2 L_p{}^2 J_v{}^2 - 16J_v{}^2 c_i DTRv^2 L_p{}^2)^{1/2} \end{aligned} \tag{17}$$

Since negative values of σ have no meaning, the positive root (root 2) is chosen.

Fritz and Whitworth (1994) derived a transient solution for the development of the concentration polarization layer and used it to describe the results of a sedimented clay membrane experiment with a lithium chloride solution. Their equation is

$$c_{(x,t)} = c_i + \left[(c_{o(t)} - c_i)/2\right] \cdot \left\{\left[\exp(-J_v x/D) - \exp(-J_v x_i/D)\right] \cdot \operatorname{erfc}\left[(x - J_v t)/(2(Dt)^{1/2})\right] + \operatorname{erfc}\left[(x + J_v t)/(2(Dt)^{1/2})\right]\right\} \quad (18)$$

which can be rearranged to solve for $c_{o(t)}$.

$$c_{o(t)} = (\bar{c}_{x,t} - c_i x_i)/\Lambda + c_i \quad (19)$$

where

$$\Lambda = \frac{1}{2}\int_{x_o}^{x_i} \left\{\left[\exp(-J_v x/D) - \exp(-J_v x_i/D)\right]\operatorname{erfc}\left[(x - J_v t)/(2(Dt)^{1/2})\right] + \operatorname{erfc}\left[(x + J_v t)/(2(Dt)^{1/2})\right]\right\} dx \quad (20)$$

We used Equation 19 to calculate c_o and then Equation 17 to calculate c_o for Fritz and Whitworth's (1994) experiment. We next used these calculated values of c_o and Equation 1 to calculate σ. To use Equation 17, we needed the value of ζ so we calculated it from equation 13 for Fritz and Whitworth's (1994) experiment which used clay from the same batch as used in the experiments described in this report. For this experiment, $\zeta = 15$. Barone et al. (1992) measured ζ for the Bison mudstone and obtained values of from 6.7 to 5.0 and Barone et al. (1990) measured obtained value of ζ of 5.0 to 10 for samples of the Queenston shale. The average of their data is approximately 7.0. The ζ value of 15 determined for Fritz and Whitworth's (1994) data is therefore reasonable. The values used in the comparison of equations 17 and 19 are given in Table 19.

Table 19. Values of parameters used in comparison of equations 17 and 19.

Parameter	Value
D	1.312×10^{-5}
c_i	9.99×10^{-6} moles/cm^3
x_i	12.67 cm
t	1663500 sec
T	295°K
Cell Concentration	11.28×10^{-6} moles/cm^3
ΔP	20.47×10^{6} dynes/cm^2
J_v	1.37×10^{-5} cm/sec
v	2 (unitless)
A	20.29 cm^2
L_P	6.92×10^{-13}

Equation 17 is not sensitive to values of ζ. Varying values of ζ as much as one order of magnitude ultimately result in changes in the value of sigma of only 0.1. The difference in steady-state c_o calculated by these two methods is only 2.4%. The difference in σ resulting from the use of these two equations to calculate c_o is 3.4 %. Therefore, there is good agreement between the two methods in spite of the fact that calculations using the transient solution of Fritz and Whitworth (1994) require the assumption that $c_{o(t)}$ does not change significantly between effluent sampling times. If equations 1 and 2 are each solved for σ, and the value of c_o from each of equations 17 and 19 is used to calculate values of σ, the value of c_o calculated by equation gives identical values of σ while Equation 19 does not. Therefore, our derivation provides a better steady-state solution to this system of simultaneous equations (equations 1 and 2) than does the transient solution of Fritz and Whitworth (1994).

Calculated values for the membrane coefficients for the experiments are given in Table 20. They were calculated using the mathematics previously described.

DISCUSSION AND MODEL DEVELOPMENT

In natural waters containing bicarbonate and carbonate alkalinity, dissolved lead concentrations should be limited by the solubility of lead carbonate (approximately 0.065 mg/l) (Hem 1959). Lead concentrations in natural groundwater seldom reach saturation for lead carbonate. However, heavy metal concentrations in contaminant plumes are often elevated over those found in pristine groundwater. For example, the concentration of lead in Wisconsin landfill leachate typically ranges from not detectable to 1.11 mg/l (Fetter 1988). Therefore, precipitation of lead minerals due to hyperfiltration through clay membranes is even more likely in polluted than undisturbed systems. The same should hold true for many other metal contaminents.

Clay membrane thickness is of critical importance because it, along with the clay's hydraulic conductivity, is a major control of the time necessary to reach steady-state. For example, Fritz and Whitworth (1994) found that a 0.3 cm thick clay membrane with a hydraulic conductivity of 2.03×10^{-10}

cm/s required a little more than 19 days to reach steady-state at a solution flux of 1.370×10^{-5} cm/s. Additionally Whitworth and Fritz (1994) found that a 0.274 cm thick clay membrane with a hydraulic

Table 20. Summary of experimental parameters for hyperfiltration experiments.

	Experiment						
Parameter	WRRI2	WRRI4	WRRI5	WRRI6	WRRI7	WRRI8	WRRI9
Starting Solution	80% $CuCO_3$	80% $CuCO_3$	80% $PbCl_2$	23% $PbCl_2$	80% $CuCO_3$	80% $CuCl_2$	80% $CoCl_2$
Final J_v (cm/s)	1.37×10^{-3}	1.37×10^{-3}	1.71×10^{-3}	1.03×10^{-3}	1.37×10^{-4}	2.06×10^{-3}	1.36×10^{-3}
Final ΔP (bars)	30.95	4.90	24.15	16.39	6.19	66.3	63.0
Clay Type	Na-Montmoril-Lonite	Na-Montmoril-lonite	Na-Montmoril-lonite	Na-Montmoril-lonite	Na-Montmoril-lonite	Na-Montmoril-lonite	Na-Montmoril-lonite
Mass of Clay (g)	0.60	0.60	0.60	0.60	0.60	0.60	0.60
L_P (cm^3/dyne·s)	4.97×10^{-11}	5.37×10^{-10}	9.00×10^{-11}	6.34×10^{-11}	2.21×10^{-11}	7.21×10^{-11}	6.69×10^{-11}
Membrane Thickness (cm)	0.064	0.064	0.097	0.094	0.061	0.094	0.094
Membrane Porosity (%)	79	79	86	85	78	86	86
Theoretical Steady-state σ	0.90	0.95	0.74	0.49	0.59	0.96	0.88
Approximate Steady-state ω (mole/dyne·s)	7.25×10^{-16}	7.25×10^{-16}	8.32×10^{-16}	8.59×10^{-16}	7.60×10^{-16}	8.89×10^{-16}	7.83×10^{-16}
c_i (moles/cm^3)	7.08×10^{-6}	3.58×10^{-6}	2.30×10^{-5}	7.38×10^{-6}	1.96×10^{-6}	2.93×10^{-5}	7.69×10^{-5}
Theoretical Steady-state c_o (mole/dyne·s)	9.27×10^{-5}	5.45×10^{-5}	1.24×10^{-4}	1.88×10^{-5}	4.35×10^{-6}	5.78×10^{-4}	7.47×10^{-4}
c_o/c_i	13.0	19.9	15.4	2.55	2.22	19.7	9.7
Temperature (°C)	22	22	21.5	21.5	22	21.5	21.5
$10D/J_v$ (cm)	0.058	0.058	0.08	0.135	0.58	0.07	0.09

Note: D calculated from Nernst Equation. D for copper carbonate = 7.963×10^{-6}, D for lead chloride = 1.454×10^{-5}, D for copper chloride = 1.43×10^{-5}, D for cobalt chloride = 1.26×10^{-5}. All membrane coefficients shown in this table are calculated for the cation.

conductivity of 1.83×10^{-16} required only about 20 days to closely approach steady-state at a solution flux of approximately 8.83×10^{-6} cm/s, and a 0.810 cm thick clay membrane with a hydraulic conductivity of 1.15×10^{-17} cm/s required approximately 90 days to closely approach steady-state. These experiments (Fritz and Whitworth 1994 and Whitworth and Fritz 1994) indicate that is should be possible for hyperfiltration through thin clay membranes to reach steady-state conditions in environmentally significant time frames.

Initial estimation of the relative importance of membrane-induced precipitation on heavy metal transport in polluted aquifers requires a few assumptions. For example, consider a 1-cm thick clay with a hydraulic conductivity of 1×10^{-7} cm/s under a hydraulic gradient of 1.0 in which 0.001 cm^3 of solution pass through 1-m^2 in one second. Assuming an aquifer porosity of 25%, then the fluid which passes through one m^2 of this membrane in one year would occupy 0.126 m^3 of aquifer. Ten years would see fluid from 1.26 m^3, and 100 years would see fluid from 12.6 m^3 of aquifer material. Thus we see that over a period of 100 years, a thin bounding clay membrane can remove much of the heavy metal from a aquifer almost 13 m thick both by precipitation due to solute-sieving effects and ion exchange of the contaminant ions with the exchangeable ions in the shale. The conclusion is then that aquifers with bounding shales may ultimately be self-cleaning of heavy metal contamination. Thicker clays will be just as effective in inducing precipitation, as long as the flux toward the membrane exceeds the ability of the solute to diffuse away from the membrane, however, it will take longer.

The experiments performed for this study prove that hyperfiltration-induced heavy metal precipitation is possible in the laboratory. However, it is important to determine the theoretical limits to geologic membrane-induced heavy metal precipitation. For this reason, we developed a steady-state analytical model of the membrane effect that can be applied to specific sites in the future.

For any given site, we can either calculate, measure, or estimate values of D, σ, K, Δ, c_i, v, and T. Except for c_o and J_v, all other parameters can be defined in terms of the first seven parameters listed. Therefore we will derive equations that allow the values of c_o and J_v to be calculated when the other parameters are known.

At first it seems that Darcy's law would suffice to calculate J_v. However, it is not that simple. Equation 1 shows that the total solution flux through the membrane increases as the differential pressure across the membrane increases and decreases with increasing osmotic pressure. If the osmotic pressure is zero, then Equation 1 reduces to a one-dimensional form of Darcy's Law

$$J_v = \frac{K\Delta P}{\rho g \Delta x} \tag{21}$$

Conversely, if osmotic pressure is significant, J_v will be less than would be predicted by Darcy's Law. We now derive from Equation 1 an approximate expression that will allow us to account for osmotic pressure in calculating J_v. Substituting Equation 3 and Equation 4 into Equation 1 yields

$$J_v = \frac{K}{\rho g \Delta x}(\Delta P - \sigma v RT(c_o - c_e) \tag{22}$$

The only unknown parameter in this equation is c_o. Solving Equation 8 for c_o and substituting the steady-state relationship $c_e = c_i$ yields

$$c_0 = \frac{-(\sigma c_i + c_i)}{\sigma - 1} \tag{23}$$

Substituting Equation 23 into Equation 22 yields

$$J_v = \frac{K}{\rho g \Delta x}(\Delta P - \sigma v RT(\frac{-(\sigma c_i + c_i)}{\sigma - 1} - c_i)) \tag{24}$$

where all parameters other than J_v are either known for a given system, or reasonable values can be assumed. Thus, the effects of osmotic pressure on a single-solute system can be calculated. As an

example, let's consider a 0.01M (230 mg/l) NaCl system in which Δx = 10 cm, σ = 0.6, v = 2, D = 1.545 x 10^{-5} sec/cm^2, ΔP = 1.861,585 dynes/cm^2 (27 psi), K = 1 x 10^{-9} cm/sec, T = 298.15°K, g = 980, R = 8.314 x 10^{-7}, and ρ = 1.0. J_v as calculated from Darcy's law (Equation 21) is 1.9 x 10^{-7} cm/sec while J_v calculated from Equation 25 is 9.9 x 10^{-8} cm/sec. Thus, we see that for this simple system, Darcy's Law has over-estimated J_v by 92 %. To use this equation, the value of σ will either have to be measured or estimated.

Now we derive an analytical expression for σ by substituting equations 3, 4, 12, and the steady-state relationships $J_s = J_v c_e$, and $c_i = c_e$, into Equation 2. This expression is

$$c_o = -c_i \cdot \frac{J_v \Delta x \zeta(1+\sigma) + 2Dv}{J_v \Delta x \zeta(\sigma - 1) - 2Dv} \tag{25}$$

Using equations 25 and 26, and Equation 7, we can now model steady-state membrane effects in aquifers with bounding shales. First we will choose an arbitrary domain (Fig 22) which consists of a 35 by 30 meter grid. The shale has a varying thickness to illustrate the results of membrane thickness on CPL development.

For each column on the grid, values of J_v and c_o were calculated and the values of c_x were calculated for each node in the column. The concentration values calculated for each node were then plotted using SURFER. The chosen parameters for the first example modeling run for a copper carbonate solution are: σ = 0.5, D = 7.963X10^{-6}, D* = D/2 (or w = 0.5), v = 2, T = 298, g = 980, ρ= 1.0, ζ= 7.0, ΔP = 35.2 cm, c_i = 1 x 10^{-8} moles/cm^3, K = 1 x 10^{-7} cm/sec. The results of this run are shown in Figure 23. Notice that the concentration contours in the sand generally parallel the shale boundary.

Where the shale is thinner, the concentration gradient within the CPL is steeper, and where the shale is thicker, the concentration gradient within the CPL is shallower. This occurs because Jv is greater for thinner shales. It is difficult to tell from Figure 23, but the steady-state value of c_o is independent of shale thickness. This implies that, due to the higher flux, steady-state will be reached adjacent to the

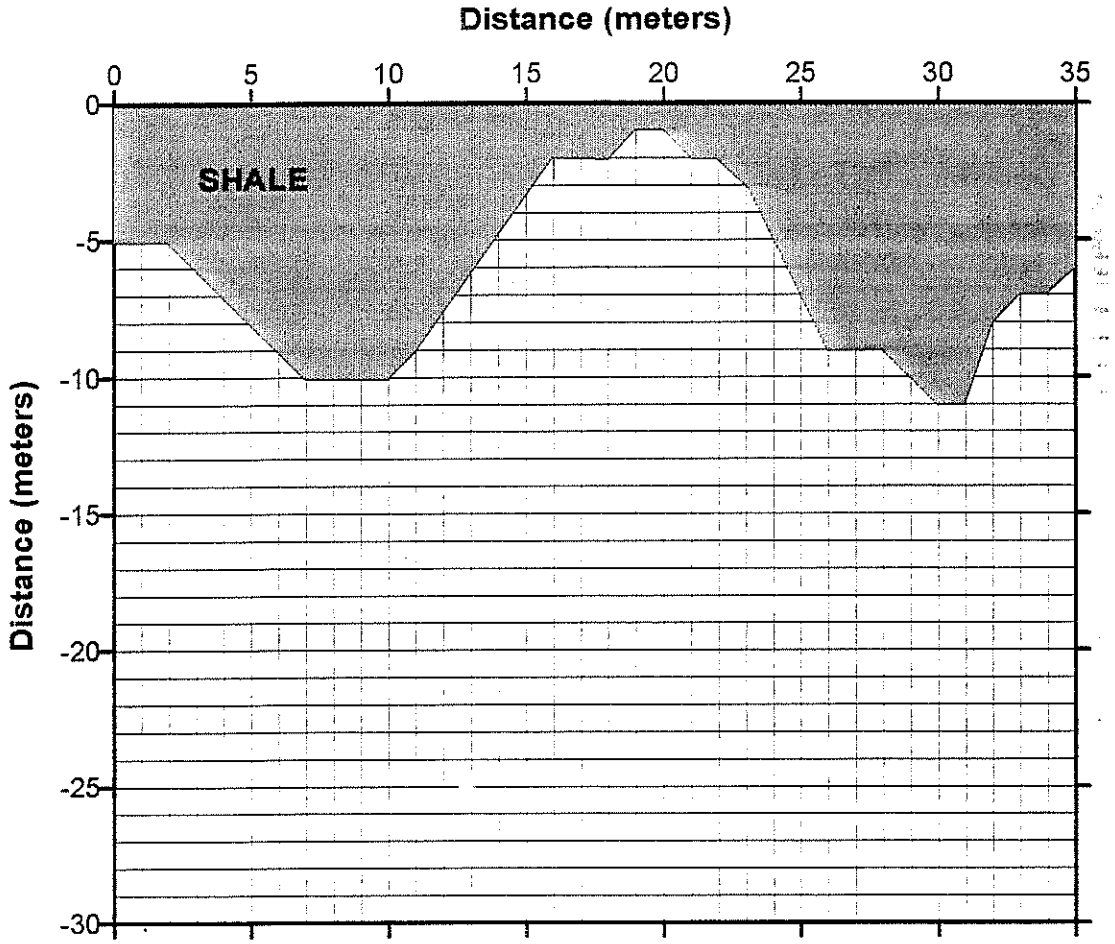

Figure 22. Domain used in modeling runs. The tinted upper portion of the diagram is the shale. Each block is 1-meter square.

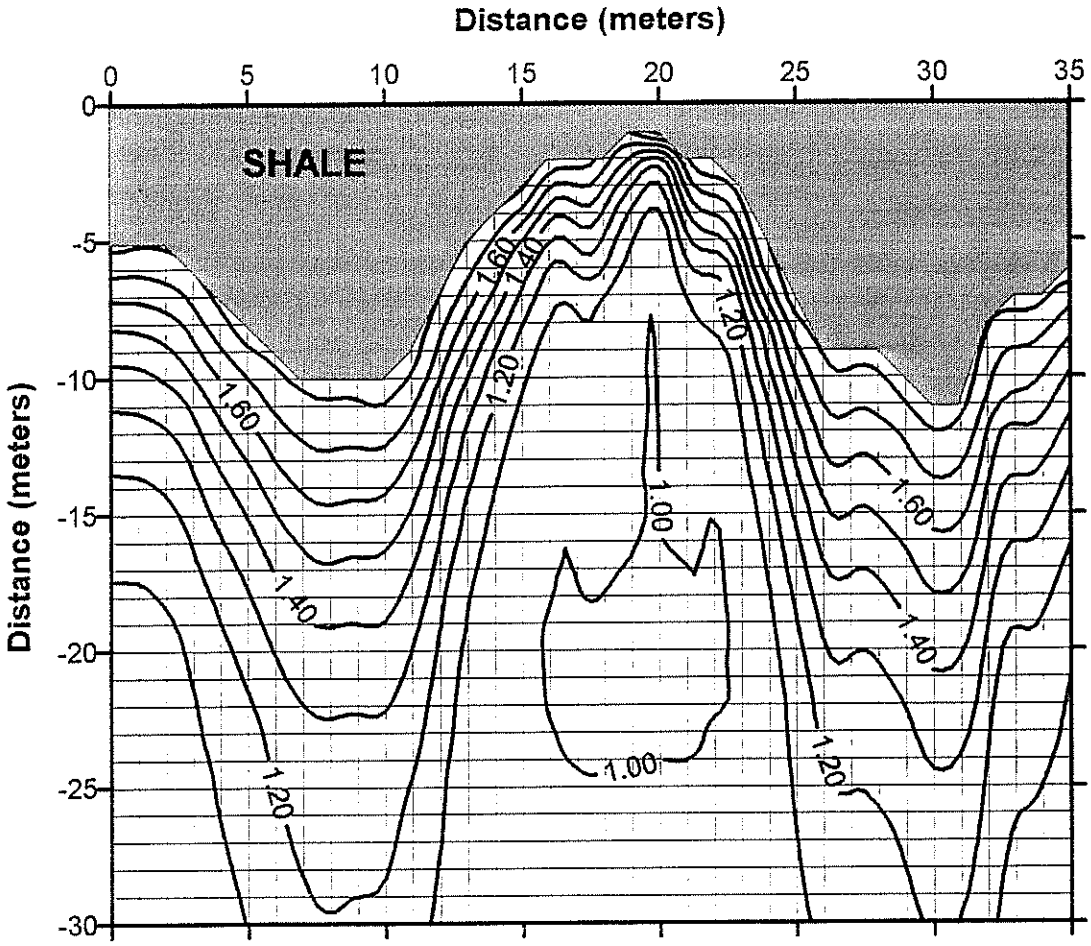

Figure 23. Results of the first modeling run. Contours represent solute concentration in moles/cm^3 x 10^{-8}.

thinner shales before it is reached adjacent to the thicker shales. For our simple example, we can assume that copper carbonate solubility is based on a Ksp of 3.2×10^{-10} (Guyon and Jones 1969) which yields a calculated solubility of 1.79×10^{-8} moles/cm^3. The calculated value of c_o in the first modeling run is 1.86×10^{-8} moles/cm^3. Therefore, the model suggests that copper carbonate should precipitate within a few centimeters of the shale membrane.

For the second modeling run all parameters are kept the same except that ΔP was increased to 140.8 cm. Notice that the increase in pressure resulted in increasing the value of c_o to 2.5×10^{-8} moles/cm^3 and pushing the 1.0×10^{-8} concentration contour closer to the shale membrane (Fig. 24). Due to the increased value of c_o, there is a wider zone of saturation adjacent to the shale membrane (Fig. 24). This suggests that higher pressures will be more efficient at developing values of c_o which rise above solubility.

It is informative to repeat this modeling run using a lower value of σ. This time the reflection coefficient is set to 0.3. Notice that the calculated value of c_o is now 1.70×10^{-8} moles/cm^3. This value is below solubility and no copper carbonate precipitation should occur (Fig. 26). Thus, when values of σ are low, precipitation is unlikely even with higher head differences across the membrane.

Groundwater systems are multi-component systems. Rewriting Equation 25 for multi-component systems yields

$$J_v = \frac{K}{\rho g \Delta x}\left(\Delta P - \sum_{0 \rightarrow j} \sigma v R T\left(\frac{-(\sigma c_{i,j} + c_{i,j})}{\sigma - 1} - c_{i,j}\right)\right) \qquad (26)$$

where the second term must be summed over all the significant solution components. It should be emphasized here that the reflection coefficient is solute-specific. Each solution component will have a different value of σ. However, these values can be measured for the solution of interest in the laboratory.

This steady-state analytical model can be modified for use with multi-component solutions and used to model membrane effects at specific contaminated sites if so desired. All that is necessary, is to account for the total osmotic effect by using Equation 27. The model will predict if heavy metal

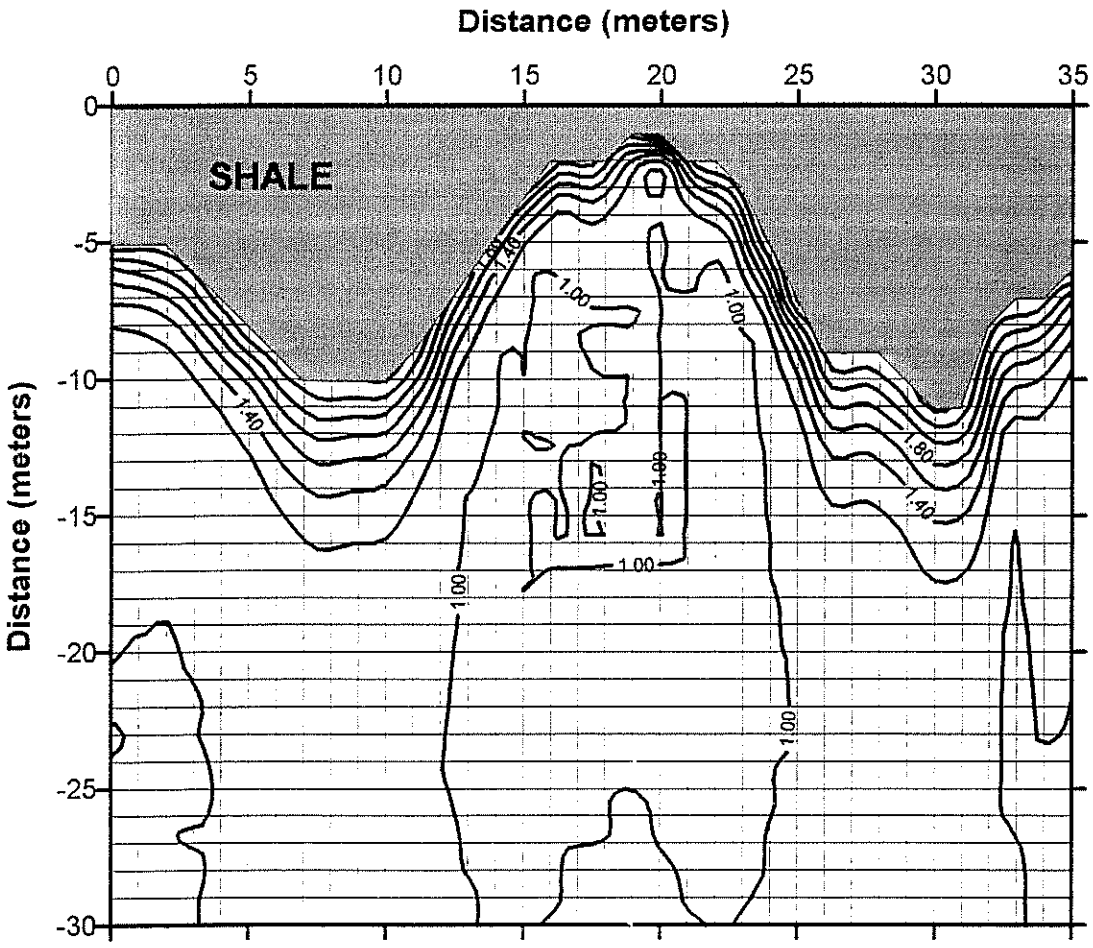

Figure 24. Results of the second modeling run. Contours represent solute concentration in moles/cm^3 x 10^{-8}

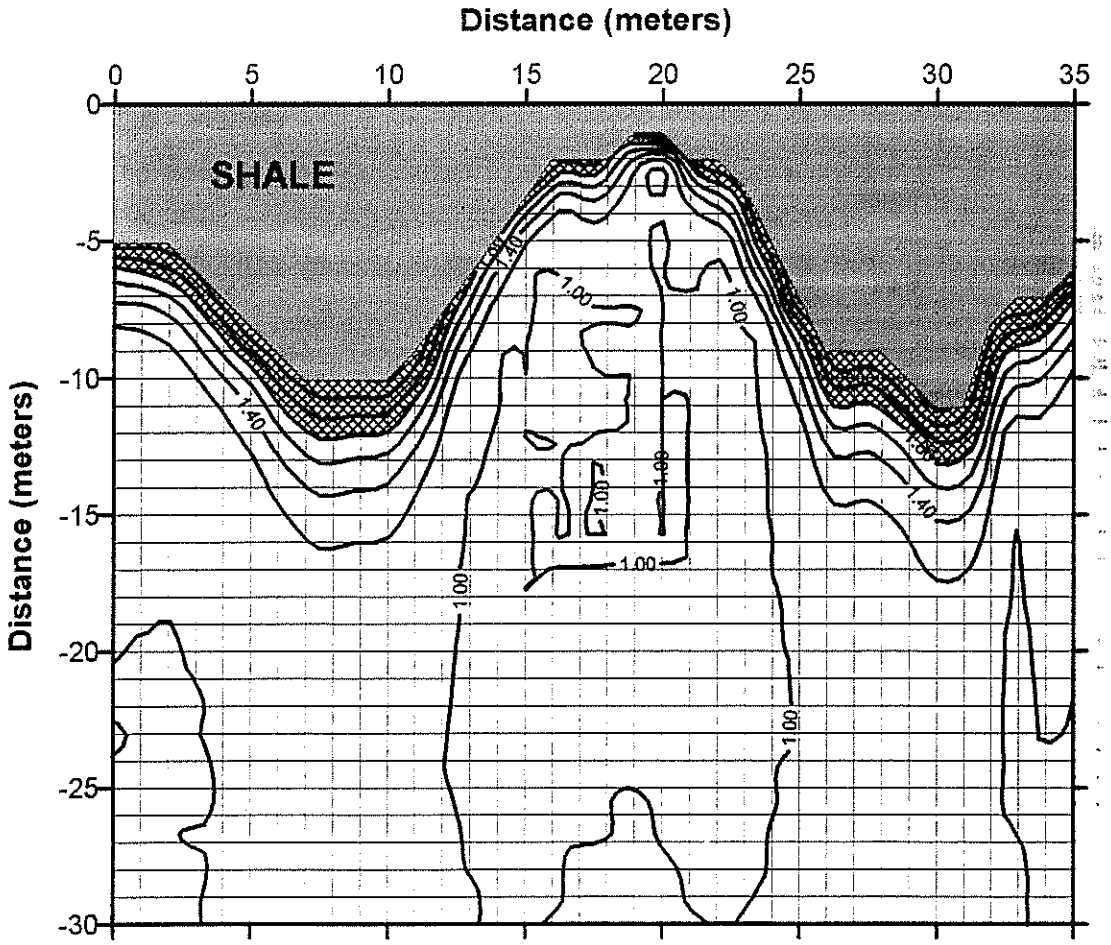

Figure 25. Results of the second modeling run showing zone of copper carbonate saturation. Contours represent solute concentration in moles/cm^3 x 10^{-8}.

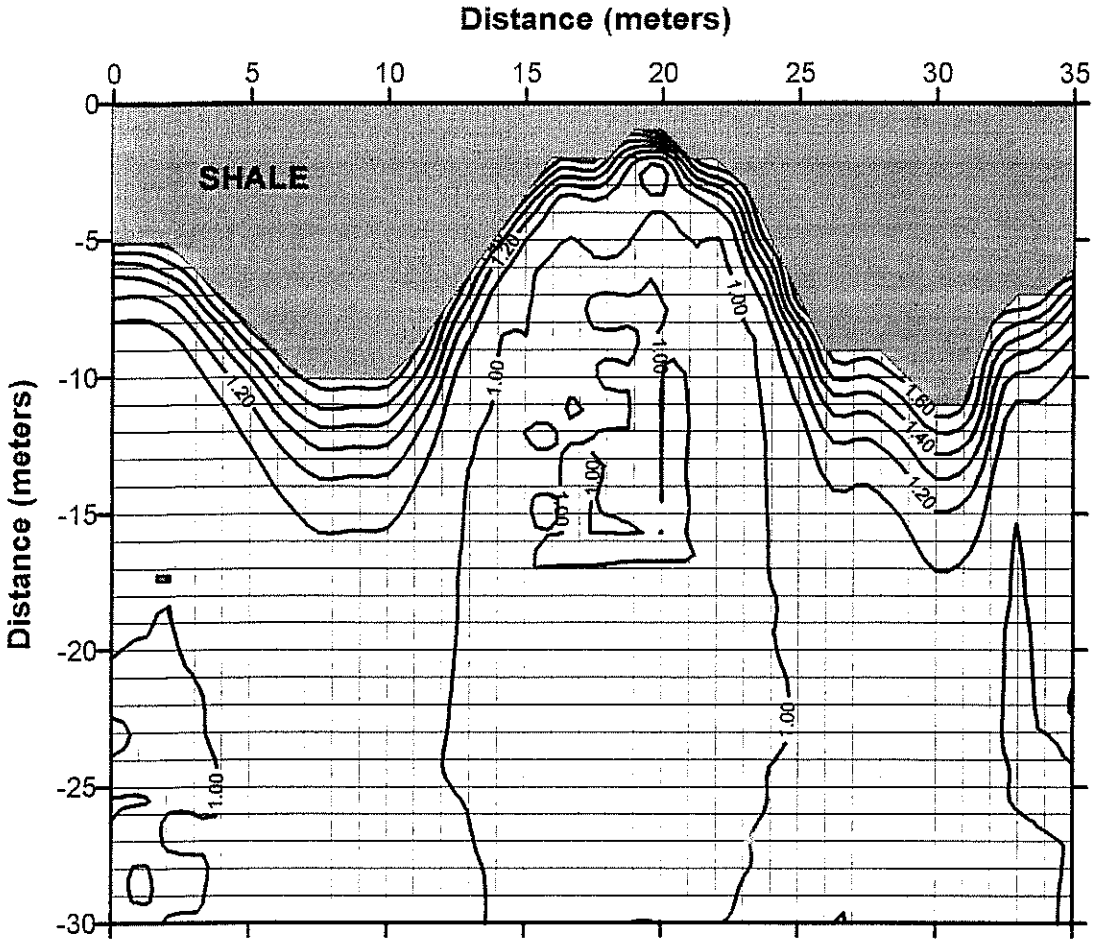

Figure 26. Results of the third modeling run. Contours represent solute concentration in moles/cm^3 x 10^{-8}

precipitation is likely, but not a precipitation rate. To be precise, if precipitation is occurring, the magnitude of the solution flux directed toward the membrane within the aquifer must be somewhat greater than the solution flux which actually passes through the membrane. However, because of the generally low concentrations involved, we can assume for purposes of illustration, that even with precipitation occurring, that the solution flux through the membrane is essentially equal to that toward the membrane within the aquifer. When precipitation does not occur, the two solute flux terms are exactly equal at steady-state.

What is the significance of membrane-induced precipitation on heavy metal contaminated plumes in the subsurface? The experiments suggest the following:

- Our experimental data suggest that heavy metals may precipitate the CPL. If, however, steady-state c_o is not greater than solubility, the result will be to increase the concentration within the CPL with no precipitation occurring. In any case, any heavy metals entering the shale membrane will be subject to ion exchange and will likely be tied up in the shale until the ion exchange capacity of the shale is exceeded.
- When heavy metal contaminant concentrations are high, the experiments suggest that the value of the reflection coefficient may still be relatively high and thus precipitation conditions may be reached in the CPL. However, under these conditions, more of the heavy metals will enter the shales. For this reason, the ion exchange capacity of the shale is more likely to be exceeded when heavy metal concentration in the aquifer are high. The assumption can be made that for a given site, any heavy metals which do not take part in precipitation and are not retained in the CPL will ultimately enter the bounding shales and be available to participate in ion exchange. The rate at which the heavy metals will enter the bounding shales is defined by the membrane properties of the shale and the vertical head conditions, solution composition and concentrations.
- Ion exchange is the substitution of one ion for another on the surface or in the interstices of a crystal. Ion exchange in clay minerals occurs because clay minerals can sorb cations and, to a lesser extent,

anions from solution. However, when exposed to a different solution, some of these sorbed ions are "exchanged" for other ions. The exchange of ions between the solution and the clay minerals does not affect the crystal structure because the exchangeable ions are held around the outside of the clay mineral structural unit. Numerous attempts to formulate a universal theory of ion exchange which would allow quantitative prediction of ion exchange have consistently failed (Sposito 1981) Xu and Harsh (1992) have developed an apparently successful model for monovalent cation selectivity, however, a unified model of ion exchange selectivity for clay minerals has still not emerged. For this reason, it is premature to attempt to develop a quantitative model of ion exchange effects associated with these experiments. This will be addressed in future studies designed to address that aspect of the shale/solute interaction.

This study addresses only single solute systems. Single solute groundwater systems seldom occur in nature. Future efforts on this topic will involve research into membrane-induced precipitation in multi-component systems and will include development of a model to predict the mass flux from solution into the precipitate during solute sieving by shales.

SUMMARY AND CONCLUSIONS

Seven hyperfiltration experiments were performed with sedimented clay membranes. Three of the experiments were with undersaturated copper carbonate solutions. Two of these experiments resulted in precipitation of copper minerals on the high-pressure membrane face. Two experiments were performed with under-saturated lead chloride solutions. Precipitation of cotunnite ($PbCl_2$) occurred at the high pressure membrane face in each experiment. In each case, yellow-green precipitate was visible on the membrane through the clear acrylic experimental cell before the end of the experiment. Two additional experiments with undersaturated solutions of $CuCl_2$ and $CoCl_2$ also resulted in visible precipitation. The experimental results prove that hyperfiltration-induced heavy metal precipitation is possible.

Calculated theoretical steady-state values for the reflection coefficient (a measure of membrane efficiency) for the experiments ranged from a minimum of 0.49 to a maximum of 0.96 Fritz and Marine (1983) state that σ is important because it is a measure of the osmotic efficiency of a membrane. Thus, a membrane with a $\sigma = 0.90$ would exhibit 90 % of the theoretically predicted osmotic pressure. Fritz and Marine (1983) calculated values of σ for a series of six experiments using bentonite clay membranes compacted to different porosities and NaCl solutions. The values of σ they determined ranged from 0.04 to 0.89. Thus the values of σ for the experiments performed in this study are in or just above the range of previously reported results. Kharaka and Berry's (1973) data shows that selectivity of clay membranes for cations is directly proportional to atomic weight. Copper and lead both have higher atomic weights than any cations previously used in sedimented clay membrane experiments. Therefore, the fact that relatively high values of σ were obtained in the experiments performed for this study is not surprising.

The mathematical model developed in this study is capable of determining if heavy-metal precipitation is likely at steady-state, although it is incapable of determining the precipitation rate at present. The value of the reflection coefficient can be measured in the laboratory, however, further work is needed to develop a routine method to determine values of the reflection coefficient for natural shales. The two litho-osmometers used in this study both proved to be slow to run.

Clay membrane thickness is of critical importance because it, along with the hydraulic conductivity of the clay, is a major control of the time necessary to reach steady-state. Fritz and Whitworth (1994) found that a 0.3 cm thick clay membrane with a hydraulic conductivity of 2.03×10^{-10} cm/s required a little more than 19 days to reach steady-state at a solution flux of 1.370×10^{-5} cm/s. Additionally Whitworth and Fritz (1994) found that a 0.274 cm thick clay membrane with a hydraulic conductivity of 1.83×10^{-16} required only about 20 days to closely approach steady-state at a solution flux of approximately 8.83×10^{-6} cm/s, and a 0.810 cm thick clay membrane with a hydraulic conductivity of 1.15×10^{-17} cm/s required approximately 90 days to closely approach steady-state. These experiments (Fritz and Whitworth 1994

and Whitworth and Fritz 1994) indicate that is should be possible for thin clay membranes to reach steady-state conditions in environmentally significant time frames. However, many natural clay or shale membranes will be thicker and will therefore require greater time to reach staedy state. Future efforts will include development of a model to predict the mass flux from solution into the precipitate during solute sieving by shales.

This study addresses only single solute systems. Single solute groundwater systems seldom occur in nature. Future efforts on this topic will involve research into membrane-induced precipitation in multi-component systems.

REFERENCES CITED

Barone, F. S., R. K. Rowe, and R. M. Quigley 1992. Estimation of chloride diffusion coefficient and tortuosity factor for mudstone. Journal of Geotechnical Engineering. 118:1031-1047.

Barone, F. S., R. K. Rowe, and R. M. Quigley 1990. Laboratory determination of chloride diffusion coefficient in intact shale. Canadian Geotechnical Journal. 27:177-184.

Bernstein, F. 1960. Distribution of water and electrolyte between homoionic clays and saturating NaCl solutions. In Clays and Clay Minerals: Proc. 8th Natl. Clay Conference. p. 122-149, Pergamon Press, Inc.

Benzel, W. M. and D. L. Graf 1984. Studies of smectite membrane behavior: Importance of layer thickness and fabric in experiments at 20°C. Geochimica et Cosmochimica Acta. 48: 1769-1778.

Berner, R. A., 1971. *Principles of chemical sedimentology*. McGraw-Hill, New York. 240 p.

Berry, F. A. F. 1960. Geologic field evidence suggesting membrane properties of shales. American Assoc. of Petroleum Geologists Bulletin. 44:953-954.

Berry, F. A. F. 1966. Proposed origin of subsurface thermal brines, Imperial Valley, California (abst.). American Assoc. of Petroleum Geologists Bulletin. 50:644-645.

Berry, F. A. F. 1967. Role of membrane hyperfiltration on origin of thermal brines, Imperial Valley, California. American Assoc. of Petroleum Geologists Bulletin. 51:454-455.

Berry, F. A. F. 1959. Hydrodynamics and geochemistry of the Jurassic and Cretaceous systems in the San Juan Basin, northeastern New Mexico and southwestern Colorado, Ph.D. dissertation, Stanford University, 192 p.

Bredehoeft, J. D., C. R. Blyth, W. A. White, and G. B. Maxey 1963. Possible mechanism for concentration of brines in subsurface formations. American Assoc. Pet. Geologists Bull. 42:257-269.

Briggs, L. J. 1902. Filtration of suspended clay from solutions. U.S. Bur. of Soils Bulletin No. 19. p. 31-39.

Campbell, D. J. 1985. Fractionation of stable chlorine isotopes during transport through semipermeable membranes. M.S. thesis, University of Arizona, 103 p.

Coplen, T. B. and B. B. Hanshaw 1973. Ultrafiltration by a compacted membrane--I. Oxygen and hydrogen isotope fractionation. Geochimica et Cosmochimica Acta. 37:2205-2310.

De Groot, S. R. and P. Mazur 1962. *Non-equilibrium thermodynamics*. North Holland Publishing Company, Holland. Also by Dover Publications, Inc., New York, 1984, 510 p.

Demir, I., 1988. Studies of smectite membrane behavior: Electrokinetic, osmotic, and isotopic fractionation processes at elevated pressures. Geochimica et Cosmochimica Acta. 52:727-737.

Domenico, P. A. and F. A. Schwartz 1990. *Physical and chemical hydrogeology*. John Wiley and Sons, New York. 824 p.

Elrick, D. E., D. E. Smiles, N. Baumgartner, and P. H. Groenvelt 1976. Coupling phenomena in saturated homo-ionic montmorillionite: I. Experimental. Soil Science Society of America Journal. 40:490-491.

Fetter, C. W. 1988. *Applied Hydrogeology*. Merrill, Columbus Ohio. 592 p.

Freeze, R. A. and J. A. Cherry 1988. *Groundwater*. Prentice-Hall, Englewood Cliffs, N. J. 604 p.

Fritz, S. J., 1992, Measuring the ratio of aqueous diffusion coefficients between $^{6}Li^{+}Cl^{-}$ and $^{7}Li^{+}Cl^{-}$ by osmometry, Geochimica et Cosmochimica Acta, v 56, 3781-3789.

Fritz, S. J., D. L. Hinz, and E. L. Grossman 1987. Hyperfiltration-induced fractionation of carbon isotopes. Geochemica et. Cosmochemica Acta. 51:1121-1134.

Fritz, S. J. and T. M. Whitworth 1994. Hyperfiltration-induced fractionation of lithium isotopes: ramifications relating to representativeness of aquifer sampling. Water Resources Research. 30:225-235.

Fritz, S. J. and T. M. Whitworth 1993. Measuring phenomenological coefficients of membranes for use in predicting osmotically-induced hydraulic pressures. Hydrological Sci. and Tech. 8:1-10.

Fritz, S. J. and C. D. Eady 1985. Hyperfiltration-induced precipitation of calcite. Geochimica et Cosmochimica Acta. 49:761-768.

Fritz, S. J. 1986. Ideality of clay membranes in osmotic processes: a review. Clays and Clay Minerals. 34:214-223.

Fritz, S. J. and I. W. Marine 1983. Experimental support for a predictive osmotic model of clay membranes. Geochimica et Cosmochimica Acta. 47:1515-1522.

Graf, D. L. 1982. Chemical osmosis, reverse chemical osmosis, and the origin of subsurface brines. Geochimica et Cosmochimica Acta. 46:1431-1448.

Graf, D. L., I. Friedman, and W. F. Meents 1965. The origin of saline pore waters, II: Isotopic fractionation by shale micropore systems. Illinois State Geological Survey Circular 393, 32 p.

Graf, D. L., W. F. Meents, I. Friedman, and N. F. Shimp, 1966. The origin of saline formation waters III: calcium chloride waters. Illinois Geological Survey Circular 397, 60 p.

Greenberg, J. A., J. K. Mitchell, and P. A. Witherspoon 1973. Coupled salt and water flows in a groundwater basin. Journal of Geophysical Research. 78:6341-6353.

Gregor, H. P. and C. D. Gregor 1978. Synthetic membrane technology. Sci. Amer. 239:112-128.

Grim, R. E. 1968. *Clay Mineralogy*. McGraw-Hill, Inc., New York. 596 p.

Guyon, J. C. and B. E. Jones 1969. *Introduction to solution equilibrium*. Allyn and Bacon, Boston. 165 p.

Hanshaw, B. B., and G. A. Hill 1969, Geochemistry and hydrodynamics of the Paradox Basin Region, Utah, Colorado, and New Mexico. Chemical Geology. 4:263-294.

Harris, F. L., G. B. Humphreys, and K. S. Spiegler 1976. Reverse osmosis (hyperfiltration) in water desalination. In P. Meares, ed., *Membrane Separation Processes*. Elsevier, Amsterdam, Chapter 4.

Haydon, P. R., and D. L. Graf 1986. Studies of smectite membrane behavior: Temperature dependence, 20-180°C. Geochemica et. Cosmochemica Acta. 50:115-121.

Hem, J. D. 1959. Study and interpretation of the chemical characteristics of natural water, U.S. Geol. Survey Water Supply Paper 1473. 269 p.

Katchalsky, A. and P. F.Curran 1965. *Biophysics*. Harvard University Press, Cambridge. 248 p.

Kedem, O. and A. Katchalsky 1962. A physical interpretation of the phenomenological coefficients of membrane permeability. Journal of General Physiology. 45:143-179.

Kemper, W. D. 1961. Movement of water as effected by free energy and pressure gradients. I. Application of classic equations for viscous and diffusive movements to the liquid phase in finely porous media. II. Experimental analysis of porous systems in which free energy and pressure gradients act in opposite directions. Proc. Soil Sci. America. 25:255-265.

Kemper, W. D. 1960. Water and ion movement in thin films as influenced by the electrostatic charge and diffuse layer of cations associated with clay mineral surfaces. Soil Science Society Proceedings, p. 10-16.

Kemper, W. D. and J. B. Rollins 1966. Osmotic efficiency coefficients across compacted clays. Soil Science Society of America. 30:529-534.

Kharaka, Y. K. and F. A. F. Berry 1973. Simultaneous flow of water and solutes through geologic membranes, I. Experimental investigation. Geochimica et Cosmochimica Acta. 37:2577-2603.

Kharaka, Y. K. and W. C. Smalley 1976. Flow of water and solutes through compacted clays. American Assoc. Pet. Geol. Bull. 60:973-980.

Kharakra, Y. K., F. A. F. Berry, and I. Friedman 1973. Isotopic compositions of oil-field brines from Kettleman North Dome, California, and their geologic implications. Geochimica et Cosmochimica Acta. 37:1899-1908.

Kohler, E. 1903. Adsorptionsprozesse als faktoren ler lagerstättenbildung und lithogenesis. Zeitschrift für praktische geologie. 11:49-59.

Lakshminarayanaiah, N. L. 1984. *Equations of membrane biophysics.* Academic Press, Inc., New York. 426 p.

Lueth, V. W. and T. M. Whitworth 1994a. Geologic membrane effects and the origin of red bed copper deposits in New Mexico (abst.). Geol. Soc. Am. Annual Meeting, Seattle, Abstracts and Programs, p A310.

Lueth, V. W. and T. M. Whitworth 1994b. Evidence of geologic membrane effects at two New Mexico red bed copper deposits (abst.), NMGS spring meeting, Socorro, NM.

Mariñas, B. J. and R. E. Selleck 1992. Reverse osmosis treatment of multicomponent electrolyte solutions. Journal of Membrane Science. 72:211-229.

Marshall, C. E. 1948. The electrochemical properties of mineral membranes III. J. Physical Chem. 52:1284-1295.

Martin, R. B. 1964. *Introduction to biophysical chemistry.* McGraw-Hill Book Company, New York. 365 p.

McKelvey, J. G. and I. H. Milne 1960. The flow of salt solutions through compacted clay. Clays and Clay Minerals. 9:248-259.

McKelvey, J. G. and I. H. Milne 1963. Permeability and salt-filtering properties of compacted clay. Clays and Clay Minerals (extended abstract). Monograph No. 13, p 250-251.

Merten, U., H. K. Lonsdale, and R. L. Riley 1964. Boundary-layer effects in reverse osmosis. I & EC Fundamentals. 3:210-213.

Mitsoyannis, E. and G. D. Saravacos 1977. Precipitation of calcium carbonate on reverse osmosis membranes. Desalination. 21:235-240.

Noggle, J. H. 1984. *Physical Chemistry.* Little, Brown & Company Limited, 953 p.

Oberg, E., F. D. Jones, H. L. Horton, and H. H. Ryffel 1992. *Machinery's Handbook*, 24th edition. Industrial Press, Inc., New York. 2543 p.

Olsen. H. W. 1972. Liquid movement through kaolinite under hydraulic, electric, and osmotic gradients. American Assoc. of Pet. Geol. Bull. 56:2022-2028.

Olsen, H. W. 1969. Simultaneous fluxes of liquid and charge in saturated kaolinite. Soil Science Society of America Proceedings. 33:338-344.

Phillips, F. M., H. M. Bentley, S. N. Davis, D. Elmore, and G. H. Swanick 1986. Chlorine 36 dating of very old groundwater 2. Milk River Aquifer, Alberta, Canada. Water Resources Research. 22:2003-2016.

Phillips, F. M. 1983. Comment on "Chemical osmosis, reverse chemical osmosis, and the origin of subsurface brines" by Graf, D. L.. Geochimica et Cosmochimica Acta. 47:1331.

Pusch, W. 1986. Measurement techniques of transport through membranes. Desalination. 59:105-198.

Shoemaker, D. P., C. W. Garland, J. I. Steinfeld, and J. W. Nibler 1981. Experiments in physical chemistry, fourth ed. McGraw-Hill Book Company, New York. 787 p.

Spiegler, K. S. and O. Kedem 1966. Thermodynamics of hyperfiltration (reverse osmosis): criteria for efficient membranes. Desalination. 1:311-326.

Soltanieh, M. and W. N. Gill 1981. Review of reverse osmosis membranes and transport models. Chemical Engineering Communications. 12:279-363.

Sourirajan, S. 1970. *Reverse Osmosis*. Academic Press, New York. 580 p.

Sposito, G. 1981. Cation exchange in soils: An historical and theoretical perspective. In Stelly, M., editor, *Chemistry in the soil environment*, American Society of Agronomy Special Publication number 40, p. 13-30.

Staverman, A. J. 1952. Non-equilibrium thermodynamics of membrane processes. Trans. Faraday Soc. 48:176-185.

Strathmann, H. and B. Kelinin 1969. Control of concentration polarization in reverse-osmosis desalination of water. Desalination. 6:179-201.

Srivastava, R. C. and A. K. Jain 1975. Non-equilibrium thermodynamics of electro-osmosis of water through composite clay membranes, 1. The electro-kinetic energy conversion. Journal of Hydrology. 25:307-324.

Walter, G. R. 1982. Theoretical and experimental determination of matrix diffusion and related solute transport properties of fractured tuffs from Nevada test site. Los Alamos National Laboratory report LA-9471-MS. 127 p.

Whitworth, T. M., G. B. Gamblin, and S. J. Fritz 1993. A Simple Air-Stream Clay Separator. Journal of Sedimentary Petrology. 66:716-718.

Whitworth, T. M. 1993. Hyperfiltration-induced isotopic fractionation: mechanisms and role in the subsurface, Ph.D. dissertation, Purdue University. 222 p.

Whitworth, T. M. and V. W. Lueth 1994. A geologic membrane mechanism for the origin of sedimentary copper deposits (abst.). New Mexico Geology. 16:36.

Whitworth, T. M., B. J. Mariñas, and S. J. Fritz 1994. Isotopic fractionation and overall permeation of lithium by a thin-film composite polyamide reverse osmosis membrane. Journal of Membrane Science. 88:231-241.

Whitworth, T. M. and S. J. Fritz 1994. Electrolyte-induced solute permeability effects in compacted smectite membranes. Applied Geochemistry. 9:533-546.

Wood, W. W. 1976. A hypothesis of ion filtration in a potable-water aquifer system. Ground Water. 14:233-244.

Wyllie, M. R. J. 1948. Some electrochemical properties of shales. Science. 108:684-685.

Wyllie, M. R. J. 1949. A quantitative analysis of the electrochemical component of the S. P. curve. J. Petroleum Tech. 1:17-26.

Xu, S. and J. B. Harsh 1992. Hard and soft acid-base model verified for monovalent cation selectivity. Soil Sci. Soc. Am. J. 54:1596-1601.

Young, A. and P. F. Low 1965. Osmosis in argillaceous rocks. American Assoc. of Pet. Geol. Bull. 49:1004-1008.